Atmos. Meas. Tech., 10, 3697–3718, 2017
https://doi.org/10.5194/amt-10-3697-2017


Atmospheric Measurement Techniques
Open Access
EGU

# Comparison of the GOSAT TANSO-FTS TIR $CH_4$ volume mixing ratio vertical profiles with those measured by ACE-FTS, ESA MIPAS, IMK-IAA MIPAS, and 16 NDACC stations

**Kevin S. Olsen[1], Kimberly Strong[1], Kaley A. Walker[1,2], Chris D. Boone[2], Piera Raspollini[3], Johannes Plieninger[4], Whitney Bader[1,5], Stephanie Conway[1], Michel Grutter[6], James W. Hannigan[7], Frank Hase[4], Nicholas Jones[8], Martine de Mazière[9], Justus Notholt[10], Matthias Schneider[4], Dan Smale[11], Ralf Sussmann[4], and Naoko Saitoh[12]**

[1]Department of Physics, University of Toronto, Toronto, Ontario, Canada
[2]Department of Chemistry, University of Waterloo, Waterloo, Ontario, Canada
[3]Istituto di Fisica Applicata "N. Carrara" (IFAC) del Consiglio Nazionale delle Ricerche (CNR), Florence, Italy
[4]Institut für Meteorologie und Klimaforschung, Karlsruhe Institute of Technology, Karlsruhe, Germany
[5]Institute of Astrophysics and Geophysics, University of Liège, Liège, Belgium
[6]Centro de Ciencias de la Atmósfera, Universidad Nacional Autónoma de México, Mexico City, Mexico
[7]Atmospheric Chemistry Division, National Center for Atmospheric Research, Boulder, CO, USA
[8]Centre for Atmospheric Chemistry, University of Wollongong, Wollongong, Australia
[9]Belgisch Instituut voor Ruimte-Aëronomie-Institut d'Aéronomie Spatiale de Belgique (IASB-BIRA), Brussels, Belgium
[10]Institute for Environmental Physics, University of Bremen, Bremen, Germany
[11]National Institute of Water and Atmospheric Research Ltd (NIWA), Lauder, New Zealand
[12]Center for Environmental Remote Sensing, Chiba University, Chiba, Japan

*Correspondence to:* Kevin S. Olsen (ksolsen@atmosp.physics.utoronto.ca)

Received: 8 January 2017 – Discussion started: 27 March 2017
Revised: 27 July 2017 – Accepted: 21 August 2017 – Published: 9 October 2017

**Abstract.** The primary instrument on the Greenhouse gases Observing SATellite (GOSAT) is the Thermal And Near infrared Sensor for carbon Observations (TANSO) Fourier transform spectrometer (FTS). TANSO-FTS uses three shortwave infrared (SWIR) bands to retrieve total columns of $CO_2$ and $CH_4$ along its optical line of sight and one thermal infrared (TIR) channel to retrieve vertical profiles of $CO_2$ and $CH_4$ volume mixing ratios (VMRs) in the troposphere. We examine version 1 of the TANSO-FTS TIR $CH_4$ product by comparing co-located $CH_4$ VMR vertical profiles from two other remote-sensing FTS systems: the Canadian Space Agency's Atmospheric Chemistry Experiment FTS (ACE-FTS) on SCISAT (version 3.5) and the European Space Agency's Michelson Interferometer for Passive Atmospheric Sounding (MIPAS) on Envisat (ESA ML2PP version 6 and IMK-IAA reduced-resolution version V5R_CH4_224/225), as well as 16 ground stations with the Network for the Detection of Atmospheric Composition Change (NDACC). This work follows an initial inter-comparison study over the Arctic, which incorporated a ground-based FTS at the Polar Environment Atmospheric Research Laboratory (PEARL) at Eureka, Canada, and focuses on tropospheric and lower-stratospheric measurements made at middle and tropical latitudes between 2009 and 2013 (mid-2012 for MIPAS). For comparison, vertical profiles from all instruments are interpolated onto a common pressure grid, and smoothing is applied to ACE-FTS, MIPAS, and NDACC vertical profiles. Smoothing is needed to account for differences between the vertical resolution of each instrument and differences in the dependence on a priori profiles. The smoothing operators use the TANSO-FTS a priori and averaging kernels in all cases. We present zonally averaged mean $CH_4$ differences between each instrument and TANSO-FTS with and without smoothing, and we examine their information content, their sensitive altitude range, their correlation, their a priori dependence, and the variability within each data set. Partial columns are calculated from the VMR vertical profiles, and their correlations are examined. We find that the TANSO-FTS verti-

cal profiles agree with the ACE-FTS and both MIPAS retrievals' vertical profiles within 4 % ($\pm \sim 40$ ppbv) below 15 km when smoothing is applied to the profiles from instruments with finer vertical resolution but that the relative differences can increase to on the order of 25 % when no smoothing is applied. Computed partial columns are tightly correlated for each pair of data sets. We investigate whether the difference between TANSO-FTS and other $CH_4$ VMR data products varies with latitude. Our study reveals a small dependence of around 0.1 % per 10 degrees latitude, with smaller differences over the tropics and greater differences towards the poles.

## 1 Introduction

The Greenhouse gases Observing SATellite (GOSAT) was developed by Japan's Ministry of the Environment (MOE), National Institute for Environmental Studies (NIES), and the Japan Aerospace Exploration Agency (JAXA), and it was launched in 2009 with an inclination of 98° (Yokota et al., 2009). The objectives of the GOSAT mission include monitoring the global distribution of greenhouse gases, estimating carbon dioxide ($CO_2$) source and sink locations and strengths, and verifying the reduction of greenhouse gas emissions as mandated by the Kyoto Protocol. GOSAT carries two instruments: the Thermal And Near infrared Sensor for carbon Observations (TANSO) Fourier transform spectrometer (FTS) and the TANSO Cloud and Aerosol Imager (TANSO-CAI). In this work we compare TANSO-FTS measurements with those made by similar instruments in order to validate its quality. Any biases in the data product need to be well understood for it to be used by other researchers, and their discovery may lead to improvements of future versions.

TANSO-CAI is a radiometer with four spectral bands that is able to measure the cloud fraction in the field of view of TANSO-FTS (Ishida and Nakajima, 2009; Ishida et al., 2011). TANSO-FTS is a nadir-viewing double-pendulum FTS, whose technical details are described in Sect. 2.1. TANSO-FTS makes observations of infrared radiation emitted from the Earth's atmosphere in four bands. Three bands are in the short-wave infrared region and are used to measure total columns of $CO_2$ and methane ($CH_4$). The fourth channel is in the thermal infrared (TIR) to provide GOSAT with sensitivity to the vertical structure of $CO_2$ and $CH_4$.

This work follows Holl et al. (2016), who compared Atmospheric Chemistry Experiment (ACE) FTS version 3.5 (v3.5) and TANSO-FTS TIR version 1 (v1) vertical profiles with those measured by a ground-based FTS at the Polar Environment Atmospheric Research Laboratory (PEARL) at 80° N in Eureka, Canada (Batchelor et al., 2009). We employ a similar methodology, extend that study globally, and include multiple ground-based FTSs that are part of the Network for the Detection of Atmospheric Composition Change (NDACC; Kurylo and Zander, 2000). Holl et al. (2016) observed that, after smoothing the ACE-FTS profiles using the TANSO-FTS averaging kernels and a priori profiles, the difference is close to 0 above 15 km but that there is a bias at lower altitudes, where TANSO-FTS retrieves more $CH_4$, with a mean excess of 20 ppbv in the troposphere. The data analyzed by Holl et al. (2016) are limited to a single location characterized by cooler temperatures and lower humidity than lower latitudes, and limited latitudinal transport. Our objective is to investigate whether the results of Holl et al. (2016) are local or hold at all latitudes and to provide additional global validation of the TANSO-FTS v1 $CH_4$ data product.

In this manuscript, we examine the TIR data product from TANSO-FTS, specifically, $CH_4$ volume mixing ratio (VMR) vertical profiles, by determining when TANSO-FTS TIR retrievals of $CH_4$ were made in coincidence with those of other satellite-borne and ground-based FTS instruments. Comparisons of satellite instruments are made with the ACE-FTS on SCISAT, described in Sect. 2.2, and the Michelson Interferometer for Passive Atmospheric Sounding (MIPAS) on the Environmental Satellite (Envisat), described in Sect. 2.3. The NDACC InfraRed Working Group (IRWG) has a network of ground-based FTSs; we used 16 that retrieve vertical profiles of $CH_4$ VMR to compare with the TANSO-FTS TIR data. The NDACC data are described in Sect. 2.4. A summary of the instruments used in this study is given in Table 1.

The question we are asking in this validation study is not, what is the magnitude of the difference between retrieved $CH_4$ vertical profiles from TANSO-FTS and other instruments, but: given the vertical resolution, information content, and a priori dependence of TANSO-FTS, would $CH_4$ vertical profile retrievals derived from another co-located instrument's measurements agree with those for TANSO-FTS? To answer this question, a smoothing operator is applied to the vertical profiles of the instruments with finer vertical resolution (and therefore finer structure in the vertical profiles). This smoothing operator, described by Rodgers and Connor (2003) and presented in Sect. 6.1, uses the a priori profiles and averaging kernels from TANSO-FTS. In this study, results with and without smoothing are presented (Sect. 6.3).

For each comparison pair, the averaging kernels, information content, and variability of the retrievals are examined in Sects. 3 and 5. The instrument with finer vertical resolution is smoothed using the averaging kernels of the instrument with coarser vertical resolution (TANSO-FTS in all cases presented here) in order to account for the structure intrinsic to a finer-resolution instrument. For each coincident pair, the absolute and relative differences of the smoothed and unsmoothed VMR vertical profiles are found, and their means, correlation coefficients, $R^2$, and numbers of coincident pairs are computed at each pressure level. For each vertical profile in a coincident pair, an overlapping vertical extent is selected using the sensitivity, or response, of the TANSO-FTS retrieval (area of the averaging kernel matrix), partial columns

**Table 1.** FTS instruments used in the $CH_4$ VMR vertical profile comparisons presented herein.

| Instrument | Spectral resolution[a] | Spectral range[b] | Viewing geometry | NDACC latitude | NDACC longitude | Reference |
|---|---|---|---|---|---|---|
| TANSO-FTS | $0.2\,cm^{-1}$ | $700–1800\,cm^{-1}$ | nadir | | | Kuze et al. (2009) |
| MIPAS | $0.0625\,cm^{-1}$ | $685–2410\,cm^{-1}$[c] | limb | | | Fischer et al. (2008) |
| ACE-FTS | $0.02\,cm^{-1}$ | $750–4400\,cm^{-1}$ | solar occultation | | | Bernath et al. (2005) |
| Eureka | $0.0024\,cm^{-1}$ | $450–4800\,cm^{-1}$ | ground | 80.1° N | 86.4° W | Batchelor et al. (2009) |
| Ny Ålesund | $0.0015\,cm^{-1}$ | $475–4500\,cm^{-1}$ | ground | 78.9° N | 11.9° E | Notholt et al. (1997) |
| Thule | $0.004\,cm^{-1}$ | $700–5000\,cm^{-1}$ | ground | 76.5° N | 68.8° W | Goldman et al. (1999) |
| Kiruna | $0.0024\,cm^{-1}$ | $450–4800\,cm^{-1}$ | ground | 67.8° N | 20.4° E | Blumenstock et al. (2006) |
| Bremen | $0.0024\,cm^{-1}$ | $450–4800\,cm^{-1}$ | ground | 53.1° N | 8.8° E | Buchwitz et al. (2007) |
| Zugspitze | $0.0015\,cm^{-1}$ | $475–4500\,cm^{-1}$ | ground | 47.4° N | 11.0° E | Sussmann and Schäfer (1997) |
| Jungfraujoch | $0.0015\,cm^{-1}$ | $475–4500\,cm^{-1}$ | ground | 46.6° N | 8.0° E | Zander et al. (2008) |
| Toronto | $0.004\,cm^{-1}$ | $750–8500\,cm^{-1}$ | ground | 43.6° N | 79.4° W | Wiacek et al. (2007) |
| Izaña | $0.0024\,cm^{-1}$ | $450–4800\,cm^{-1}$ | ground | 28.3° N | 16.5° W | Schneider et al. (2005) |
| Mauna Loa | $0.0024\,cm^{-1}$ | $450–4800\,cm^{-1}$ | ground | 19.5° N | 155.6° W | Hannigan et al. (2009) |
| Altzomoni[d] | $0.0024\,cm^{-1}$ | $450–4800\,cm^{-1}$ | ground | 19.1° N | 98.7° W | Baylon et al. (2014) |
| St. Denis, Réunion | $0.0036\,cm^{-1}$ | $600–4300\,cm^{-1}$ | ground | 20.9° S | 55.5° E | Senten et al. (2008) |
| Maïdo, Réunion[e] | $0.0024\,cm^{-1}$ | $600–4500\,cm^{-1}$ | ground | 21.1° S | 55.4° E | Baray et al. (2013) |
| Wollongong | $0.0024\,cm^{-1}$ | $450–4800\,cm^{-1}$ | ground | 34.4° S | 150.9° E | Kohlhepp et al. (2012) |
| Lauder | $0.0035\,cm^{-1}$ | $700–4500\,cm^{-1}$ | ground | 45.0° S | 169.7° E | Bader et al. (2017) |
| Arrival Heights | $0.0035\,cm^{-1}$ | $750–4500\,cm^{-1}$ | ground | 77.8° S | 166.6° E | Wood et al. (2002) |

[a] For NDACC instruments, the best achievable spectral resolution is listed here. Operationally achieved spectral resolutions for NDACC instruments may be coarser. [b] NDACC instruments use optical filters that reduce the effective spectral range when making measurements. [c] MIPAS' spectral resolution is divided into four narrower bands. [d] The Altzomoni site came online in late 2012. [e] The Maïdo, Réunion site came online in early 2013.

are computed over this range, and their correlations are examined. Finally, this altitude range is used to estimate the mean VMR difference taken over the vertical range for each coincident pair of profiles. This data set shows any biases related to latitude, or any other parameters of the TANSO-FTS retrieval, such as incidence angle or surface type (land or water).

Section 4 describes the methods and criteria for determining coincident measurements between TANSO-FTS and each instrument. Section 6.1 provides a detailed description of the comparison methodology. Comparison results for each instrument are presented in Sect. 6.2. The satellite instruments are zonally averaged, and each NDACC site is shown. Partial column calculation methodology is presented in Sect. 7.1, and correlation results are shown in Sect. 7.2. A discussion follows in Sect. 8, focusing on our investigation of biases within the TANSO-FTS retrievals related to latitude and other parameters.

## 2 Data sets

### 2.1 TANSO-FTS

TANSO-FTS makes measurements of radiance in four bands; the TIR band is between 700 and $1800\,cm^{-1}$ and is used to retrieve vertical profiles of $CH_4$ VMRs. TANSO-FTS has a spectral resolution of $0.2\,cm^{-1}$ and operates in a nadir- or near-nadir-viewing geometry (Kuze et al., 2009). To improve coverage, its field of view sweeps longitudinally, and TANSO-FTS makes several measurements along each cross track: five measurements prior to August 2010 and three since then (Kuze et al., 2012). This leads to TANSO-FTS having the highest density of measurements and greatest spatial coverage among the instruments considered herein.

Retrievals of v1 $CH_4$ follow the nonlinear maximum a posteriori method used for v1 $CO_2$ presented in Saitoh et al. (2009, 2016). They are performed on a fixed pressure grid, and the pressure levels are adjusted based on the averaging kernels for the retrieval. In the v1 retrieval algorithm, water vapour, nitrous oxide, ozone concentrations, temperature, surface temperature, and surface emissivity were retrieved simultaneously with $CH_4$ concentration from V161.160 L1B spectra. A priori data are based on simulated data from the NIES transport model (TM; Maksyutov et al., 2008; Saeki et al., 2013), and the retrievals use the HITRAN 2008 line list (Rothman et al., 2009) with several updates up to 2011 (Saitoh et al., 2009).

An initial comparison of TANSO-FTS v1 to a single NDACC station, Eureka, and to ACE-FTS measurements made in the Arctic within a quadrangle surrounding PEARL

(60–90° N and 120–40° W) has been recently made (Holl et al., 2016). The v1 $CH_4$ product was also compared globally with the version 6 $CH_4$ data product from the Atmospheric Infrared Sounder (AIRS) on Aqua (Zou et al., 2016).

### 2.2 ACE-FTS

ACE-FTS was launched into low Earth orbit in 2003 on board the Canadian Space Agency's (CSA's) SCISAT. The scientific objectives of ACE are to study ozone distribution in the stratosphere, the relationship between atmospheric chemistry and climate change, the effects of biomass burning on the troposphere, and the effects of aerosols on the global energy budget (Bernath, 2017).

ACE-FTS is a high-resolution, double-pendulum FTS with a spectral resolution of $0.02\,cm^{-1}$ that covers a broad spectral range between 750 and $4400\,cm^{-1}$. It operates in solar occultation mode, making a series of measurements for tangent altitudes down to 5 km (or cloud tops) at local sunrise and sunset along its orbital path (Bernath et al., 2005). Its Level 2 data products are vertical profiles of temperature, pressure, and the VMRs of 36 trace gases, as well as isotopologues of major species, reported on an altitude grid at the measurement tangent altitudes or interpolated onto a 1 km grid. Retrievals of the version 2.2 (v2.2) data product are described in Boone et al. (2005), and updates regarding the latest release, version 3.5 (v3.5), are described in Boone et al. (2013). V3.5 retrievals, with the data quality flags (v1.1) described in Sheese et al. (2015), are used herein.

When performing trace gas retrievals, tangent altitudes for each observation and vertical profiles of temperature and pressure are also retrieved using spectral fitting (not simultaneously). Comparisons with TANSO-FTS are made on a pressure grid using the retrieved pressure values at the ACE-FTS measurement heights. A priori temperature and pressure for ACE-FTS are derived from the NRLMSISE-00 model (MSIS; Picone et al., 2002) and from meteorological data provided by the Canadian Meteorological Centre with their Global Environmental Multiscale (GEM) model (Côté et al., 1998). Fitted spectra are computed using the HITRAN 2004 spectral line list (Rothman et al., 2005) with modifications described in Boone et al. (2013).

Validation of v2.2 $CH_4$ VMR vertical profiles is presented in de Mazière et al. (2008) and was performed using several ground-based FTSs that are part of NDACC, as well as one at Poker Flat. For that comparison, partial columns were computed from the ACE-FTS $CH_4$ profiles, and the correlation between partial columns computed from ground-based FTSs and from ACE-FTS was investigated. Validation was also done against the balloon-borne SPIRALE (Spectroscopie Infra-Rouge d'Absorption par Lasers Embarqués), the Halogen Occultation Experiment (HALOE) on the Upper Atmosphere Research Satellite, and MIPAS. de Mazière et al. (2008) determined that the ACE-FTS v2.2 $CH_4$ data are accurate to within 10 % in the upper troposphere and lower stratosphere and to within 25 % at high altitudes. More recently, Jin et al. (2009) compared $CH_4$ from the Canadian Middle Atmosphere Model (CMAM) with measurements from ACE-FTS, the Sub-Millimeter Radiometer (SMR) on Odin, and the Microwave Limb Sounder (MLS) on Aura, and they found agreement with ACE-FTS within 30 %. Updates to the ACE-FTS validation effort using v3.0 data and a description of the differences between v2.2 and v3.0 are presented in Waymark et al. (2013). Waymark et al. (2013) found a slight reduction in $CH_4$ VMR in the v3.0 data near 23 km and a larger reduction of around 10% between 35 and 40 km.

### 2.3 MIPAS

MIPAS is a limb-sounding FTS that was placed in polar low Earth orbit in 2002 on board the European Space Agency's (ESA's) Envisat. MIPAS aimed to provide global observations, during both night and day, of changes in the spatial and temporal distributions of long- and short-lived species, temperature, cloud parameters, and radiance. The instrument was intended to have a maximum spectral resolution of $0.025\,cm^{-1}$ (Fischer et al., 2008), but the slide system for the interferometer mirrors encountered a problem in 2004, and observations used in this study were made with a reduced effective spectral resolution of $0.0625\,cm^{-1}$ but with finer vertical sampling. Further complications arose in 2012, and ESA lost communication with Envisat, ending the mission.

The spectral range of MIPAS is 685–2410 $cm^{-1}$, allowing the retrieval of multiple trace gases. MIPAS spectra are processed independently by four research groups (Raspollini et al., 2014). In this paper, we consider two: the ESA operational analysis and the Karlsruhe Institute of Technology Institute of Meteorology and Climate Research (IMK) and the Instituto de Astrofísica de Andalucía (IAA) analysis, both described in the following subsections.

#### 2.3.1 ESA MIPAS

We use MIPAS Level 2 Prototype Processor version 6 (ML2PP v6) of the ESA operational analysis. Early versions of the ESA MIPAS gas retrievals are described in Raspollini et al. (2006) (full-resolution Instrument Processing Facility version 4.61; IPF v4.61), and the ML2PP v6 upgrades and reduced-resolution adaptations are described in Raspollini et al. (2013). Retrievals are made using a global fitting scheme followed by a posteriori Tikhonov regularization with self-adapting constraints (Raspollini et al., 2013). The ML2PP v6 data provide retrieved VMR vertical profiles of 10 atmospheric gases between approximately 6 and 70 km. Temperature and pressure are retrieved from the spectra at each tangent point of a limb scan, and a corresponding altitude grid is built from the lowest engineering tangent altitude using the equation of hydrostatic equilibrium. Initial guesses for vertical profiles of a target trace gas, tem-

perature, and interfering species are the weighted average of the results from the previous scan, an appropriate merging of IG2 (initial guess 2) climatological profiles (Remedios et al., 2007) and, if available, data from the European Centre for Medium-range Weather Forecasts (ECMWF). Spectra are computed using a specialized line list derived from HITRAN 1996 (Rothman et al., 1998).

The IPF v4.61 $CH_4$ data product has been validated by Payan et al. (2009) against four balloon instruments; including SPIRALE; three aircraft instruments; six ground-based FTSs (all are considered herein), and HALOE. They found good agreement with a 5 % positive bias in the lower stratosphere and upper troposphere. ML2PP v6 $CH_4$ was compared with BONBON air sampling measurements by Engel et al. (2016). The reduced-resolution $CH_4$ measurements (2005–2012) agree with in situ data within 5–10 %. $CH_4$ (and $N_2O$) from ESA MIPAS has been assimilated by the BASCOE code, and the assimilated products have been compared with MLS and ACE-FTS (Errera et al., 2016). The analysis has proven the high quality of the MIPAS data, but it has also identified the presence of some outliers, especially in the tropical lower stratosphere, and some discontinuities due to issues in the measurements.

#### 2.3.2 IMK-IAA MIPAS

The IMK-IAA MIPAS retrieval algorithm has been developed to include and account for deviations from local thermal equilibrium. The data presented here are IMK-IAA reduced-resolution version V5R_CH4_224/225. The early retrieval algorithms are described by von Clarmann et al. (2009), and the updates made to the current version are described by Plieninger et al. (2015). Temperature and tangent altitude are retrieved from the spectra, and pressure is computed from the equation of hydrostatic equilibrium. V5R_CH4_224/225 uses the HITRAN 2008 line list (Rothman et al., 2009). Temperature a priori profiles are determined from ECMWF analyses and MIPAS engineering information. The IMK-IAA retrieval uses Tikhonov first-order regularization in combination with an all-zero $CH_4$ a priori profile, which serves to smooth the profiles.

Validation of the IMK-IAA MIPAS V5R_CH4_222/223 data has been presented in Laeng et al. (2015). They compare data against ACE-FTS, HALOE, the MkIV balloon FTS, the Solar Occultation For Ice Experiment (SOFIE) on the Aeronomy of Ice in the Mesosphere (AIM) satellite, the SCanning Imaging Absorption spectroMeter for Atmospheric CHartographY (SCIAMACHY) on Envisat, and a cryogenic whole-air sampler (collects gas bottle samples during aircraft flights). They found an agreement within 3 % in the upper stratosphere with other satellite instruments, but in the lower stratosphere (below 25 km) a high bias was found in the MIPAS retrievals of up to 14 %. The V5R_CH4_224/225 has more recently been validated by Plieninger et al. (2016), using ACE-FTS, HALOE, and SCIAMACHY. They found MIPAS $CH_4$ retrievals to be larger by around 0.1 ppmv below 25 km, or around 5 %.

### 2.4 NDACC

NDACC is a global network of a variety of instruments that provides measurements of tropospheric and stratospheric gases that are directly self-comparable (Kurylo and Zander, 2000). The network consists of over 70 stations sparsely distributed at all latitudes. Information about NDACC is available at www.ndacc.org. In this work, we only consider a small subset of NDACC stations that feature high-resolution FTSs and provide a $CH_4$ VMR vertical profile data product via the NDACC database. Sepúlveda et al. (2012, 2014) demonstrated the good quality of $CH_4$ profiles that can be retrieved from the NDACC FTS measurements. The stations are listed in Table 1, along with their locations, spectral range and resolution, and references.

The stations do not use identical instruments, spectroscopic lines, or retrieval methods. All but one station use a version of a Bruker 120/5 M or HR and have predominantly adopted, or upgraded to, the Bruker 125HR. Some stations have more than one instrument, and the type of instrument has changed over time at many of the stations. Toronto, 43.6° N, uses a Bomem DA8.

Retrievals are generally performed using either PROFFIT (Hase et al., 2004) or SFIT4 (Pougatchev et al., 1995) following harmonized retrieval settings recommended by the NDACC IRWG (Sussmann et al., 2011, 2013). Data used herein are from the NDACC database. A summary of retrieval settings is provided by Bader et al. (2017). Lauder and Arrival Heights, at 45.0 and 77.8° S, respectively, use a retrieval strategy that adheres to that defined in Sussmann et al. (2011), with a relaxed Tikhonov regularization constraint at Arrival Heights due to the characteristic atmospheric dynamics over Antarctica. Jungfraujoch, at 46.6° N, uses SFIT2. It has been established within the NDACC IRWG that the regularization strength of the $CH_4$ retrieval strategy should be optimized so that the number of degrees of freedom for signal (DOFS) is limited to approximately 2 (Sussmann et al., 2011).

## 3 Data set variability

To provide context for the VMR differences found when comparing each instrument to TANSO-FTS, shown in Sect. 6, we have examined the variability of retrievals made for each instrument. We are interested in determining whether the mean differences found when comparing TANSO-FTS to another instrument are comparable to the differences found when comparing pairs of retrievals for a single instrument. Each pair of observations compared in this study is made at different times and locations and subject to instrument noise and analysis errors. Examining the variabil-

ity within each data set provides an indication of the magnitude of these effects. Because the observation geometries and rates of spectral acquisition are different for each instrument, our internal comparisons differ for each instrument. For example, TANSO-FTS and MIPAS have a much higher data density than ACE-FTS, which only makes two sets of observations per orbit.

Following Holl et al. (2016), we are aware that TANSO-FTS $CH_4$ retrievals are dependent on the a priori used, especially at high altitudes. TANSO-FTS vertical profiles tend to be similar to their a priori and, therefore, to each other. To provide context for our validation results, we computed the magnitude of the mean differences between the TANSO-FTS retrievals and their a priori. This is indicative of the instrument sensitivity discussed in Sect. 5 and shows by how much the retrievals deviate from the a priori. We examined 3000 randomly selected TANSO-FTS measurements by interpolating the a priori and retrieved profiles to the pressure grid used in our comparisons (Sect. 6.1) and then computed the difference between the retrieval and the a priori at each pressure level, and their mean and standard deviation. Figure 1 shows the mean $\pm 1$ standard deviation of the difference between the TANSO-FTS $CH_4$ retrievals and their corresponding a priori profiles. The peak value is 30 ppbv near 10 km ($\sim 1.5\,\%$) with a standard deviation of the same magnitude.

To examine the variability of the ACE-FTS $CH_4$ data product, we compared each retrieved profile from an ACE-FTS sunset/sunrise (occultation direction) to that from the next orbit, taking care to avoid a comparison between sunset and sunrise occultations (which are in different hemispheres), or when an acquisition was not recorded during a subsequent orbit. Considering all sunset occultations in 2011, there were 1402 retrieved vertical profiles,and 820 sequential pairs. These pairs are separated by 97 min and have a mean spatial separation of $1180 \pm 20$ km, depending on the latitude of the measurement. For each pair, we computed the VMR difference on the ACE-FTS 1 km tangent altitude grid and then found the mean and standard deviation, which are shown in Fig. 1. Within the ACE-FTS data, the largest systematic variability ($-4$ ppbv) occurs around 30 km, with extreme outliers being observed at the lowest tangent altitudes. The mean magnitude of the ACE-FTS variability is 2 ppbv (0.1 %) at all altitudes and 9 ppbv below 15 km (0.4 %).

To examine the variability of the MIPAS data sets, we compared the vertical profiles retrieved by IMK-IAA and ESA that were made from the same MIPAS limb observations and within our coincident data set. This provides an indication of the impact of different retrieval algorithms on retrieved profiles. For each pair of retrieved vertical profiles from a single set of MIPAS spectra, we interpolated the ESA retrieval to the IMK-IAA 1 km grid and computed their difference (IMK-IAA $-$ ESA), and then found the mean and standard deviation. Figure 1 shows the mean $\pm 1$ standard deviation for this comparison. The two retrievals show good

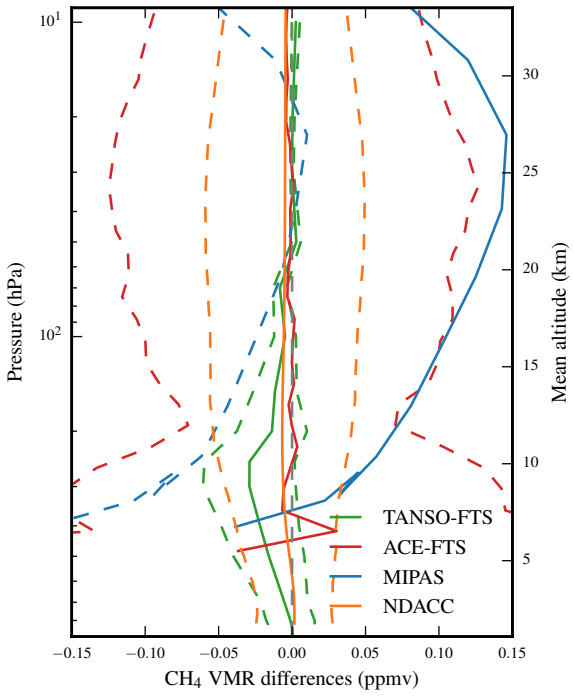


**Figure 1.** Results for investigating the variability within each $CH_4$ VMR profile data set. Shown are the following comparisons: TANSO-FTS retrievals compared to their a priori (green), pairs of sequential ACE-FTS retrievals (red), ESA MIPAS retrievals compared to IMK-IAA MIPAS retrievals made for the same limb observations (blue), and pairs of NDACC retrievals made on the same day (orange). All retrieved profiles used are coincident with TANSO-FTS. Dashed lines are 1 standard deviation.

agreement above 30 km (not shown), while the IMK-IAA data have a positive bias relative to the ESA data product of around 0.15 ppmv between 20 and 30 km. This bias is consistent with the validation results presented in Laeng et al. (2015). The ESA and IMK-IAA comparison exhibits the largest variability, with a mean magnitude (mean of absolute values) of 50 ppbv (2 %) for the altitude range considered (9–34 km). Since the two products use the same spectra, it is possible that part of the internal instrument variability is hidden in this approach.

To investigate the variability of the NDACC data, we compared pairs of observations made at an NDACC site on the same day. We considered only NDACC $CH_4$ VMR vertical profiles that were in coincidence with TANSO-FTS. For each pair of NDACC measurements, we computed the $CH_4$ VMR differences on the standard NDACC retrieval grid (earlier profile minus later profile; if there are multiple coincidences in a day, differences are found relative to the earliest). The mean and standard deviation of these differences are also shown in Fig. 1. When examining several measurements from the same day, the NDACC differences show a systematic mean increase in tropospheric $CH_4$ with time during a single day. This variability is small, however, with a mean

of −4 ppbv below 30 km and a peak at 12 km of −6 ppbv (0.3 %).

Our variability investigation found that the ACE-FTS data exhibit the smallest variability between measurements, that MIPAS exhibits the largest, and that NDACC and TANSO-FTS are of similar magnitudes. The magnitude of the internal variability of the data sets is between ±2 ppbv (e.g., for NDACC and ACE-FTS in the upper troposphere) and ± 3 ppbv, or around 2 % (e.g., for TANSO-FTS and the lower limits of ACE-FTS).

## 4 Coincidences

Due the coverage and data collection rates of each instrument, different coincidence criteria were used. ACE-FTS has an inclination of 74° and operates in solar occultation mode, recording only two occultations per orbit, predominantly at high latitudes; the NDACC sites are stationary; MIPAS makes frequent observations at all latitudes; and the spatial distribution of TANSO-FTS observations is enhanced by its cross-track observation mode. In the case of ACE-FTS and NDACC stations, the objective of the coincidence criteria was to maximize the number of measurements used. Conversely, in the case of MIPAS, the objective was to reduce the number of potential coincident measurements. For ACE-FTS and NDACC, we sought measurements made within 12 h and within 500 km of each TANSO-FTS measurement (spatial separation calculated using the Vincenty method (Vincenty, 1975)). For the MIPAS data sets, we sought measurements made within 3 h and 300 km. When searching for MIPAS–TANSO-FTS coincidences within 12 h and 500 km, we find approximately 180 000 coincidences per month.

The criteria used in this study are comparable to previous $CH_4$ studies. For example, de Mazière et al. (2008) used criteria of 24 h and 1000 km when comparing ACE-FTS $CH_4$ to ground sites, and 6 h and 300 km when comparing ACE-FTS to MIPAS. Payan et al. (2009) used criteria of 3 h and 300 km when comparing MIPAS $CH_4$ to ground- and satellite-based spectrometers. Laeng et al. (2015) used criteria of 9 h and 800 km when comparing MIPAS $CH_4$ to ACE-FTS, and 24 h and 1000 km when comparing MIPAS to HALOE.

TANSO-FTS $CH_4$ VMR vertical profiles tend not to be sensitive above the upper troposphere (see Sect. 5), while ACE-FTS and MIPAS retrievals have a limited vertical extent in the troposphere. To ensure that measurements made by each instrument overlap, a restriction was placed on ACE-FTS and MIPAS measurements: that their retrieved vertical profiles extend to low enough altitudes, after applying data quality criteria. For ACE-FTS, this requirement was 10 km. For MIPAS, this requirement was relaxed to less than 12 km. IMK-IAA MIPAS $CH_4$ VMR vertical profile retrievals do not extend as low as those made by ESA, to the extent that having the same restriction on altitude range results in only a quarter as many coincidences as the ESA data product. Relaxing the constraint to only 12 km maintains the assurance that retrieved VMRs will overlap with the TANSO-FTS altitude range, though there are only 60 % as many IMK-IAA coincidences as ESA coincidences.

TANSO-FTS makes nadir observations in a grid pattern by sweeping its line of sight across its ground-track. This results in a high density of vertical profiles, such that – for a single observation made by ACE-FTS, MIPAS, or NDACC – there are an average of 11 coincident TANSO-FTS measurements. The subsequent measurement made by MIPAS or an NDACC station will be coincident with a similar number of TANSO-FTS measurements, and most of those will also be coincident with the previous MIPAS or NDACC measurement. A common way to deal with multiple coincidences is to take the mean of the VMR vertical profiles from each instrument and to compute the difference of the means (e.g., Holl et al., 2016). When comparing MIPAS to TANSO-FTS, however, this results in some measurements contributing to the analysis more times than others, biasing the computed VMR difference profiles. Furthermore, this leads to using a mean TANSO-FTS VMR vertical profile that is strongly smoothed, while a coincident ACE-FTS (or NDACC, depending on the station's rate of acquisition at the time) VMR vertical profile is not.

To reduce biases caused by over-counting, when comparing TANSO-FTS to MIPAS, and by smoothing, when comparing TANSO-FTS to ACE-FTS, we reduced the number of coincident measurements by seeking a set of one-to-one coincidences for unique measurements in the sparser data set (which is always ACE-FTS, MIPAS, or NDACC). For each measurement that is being compared to TANSO-FTS, we find the TANSO-FTS measurement with the minimum of the sum of ratios of distance in space and time to the coincidence criteria, giving equal weight to both parameters as $\min(\mathrm{d}x/x_{\mathrm{crit}} + \mathrm{d}t/t_{\mathrm{crit}})$, where $\mathrm{d}x$ and $\mathrm{d}t$ are the distance and time between a given measurement and a TANSO-FTS coincidence, and $x_{\mathrm{crit}}$ and $t_{\mathrm{crit}}$ are the coincidence criteria. This method is similar to using a standard score to compare the spatial and temporal separation, but the sample size of the set of TANSO-FTS measurements coincident with another measurement is on the order of only 10. Furthermore, the mean and standard deviations of $\mathrm{d}x$ and $\mathrm{d}t$ reflect the time and distance between each consecutive TANSO-FTS measurement, rather than the time and spatial separation between each TANSO-FTS measurement and those from MIPAS, ACE-FTS, or NDACC.

Table 2 shows the total number of coincidences found between TANSO-FTS and each validation target instrument, as well as the subsets of unique TANSO-FTS measurements and the one-to-one coincidences used in this paper (equivalent to the number of unique measurements made by each target instrument). Figure 2 shows an example of the global distribution of coincident measurements. Shown are the first 200 one-to-one coincidences after 1 January 2012. For the ESA and IMK-IAA MIPAS data products, this number of

**Table 2.** Number of coincident $CH_4$ VMR vertical profile measurements that were found between TANSO-FTS retrievals and those from ESA MIPAS, IMK-IAA MIPAS, ACE-FTS, and NDACC stations. The three columns show the total number of coincidences found, the number of unique TANSO-FTS measurements within those coincidences, and the size of the reduced one-to-one coincidences used.

| Target instrument | Total coincident profiles | Unique TANSO-FTS profiles | One-to-one profiles used |
|---|---|---|---|
| ESA MIPAS | 450 230 | 358 267 | 85 386 |
| IMK-IAA MIPAS | 267 065 | 210 573 | 51 099 |
| ACE-FTS | 51 937 | 47 560 | 4302 |
| Total NDACC | 213 181 | 44 920 | 17 637 |
| Eureka | 11 843 | 2447 | 1009 |
| Ny Ålesund | 5445 | 1300 | 349 |
| Thule | 6997 | 3359 | 513 |
| Kiruna | 4595 | 2056 | 529 |
| Bremen | 2610 | 1452 | 211 |
| Zugspitze | 47 512 | 5743 | 3469 |
| Jungfraujoch | 18 757 | 5938 | 1493 |
| Toronto | 9909 | 5195 | 816 |
| Izaña | 56 254 | 4336 | 4501* |
| Mauna Loa | 4338 | 2381 | 379 |
| Altzomoni | 4746 | 854 | 486 |
| St. Denis, Réunion | 12 270 | 3161 | 1507 |
| Maïdo, Réunion | 3139 | 868 | 383 |
| Wollongong | 27 781 | 4808 | 2365 |
| Lauder | 7083 | 2638 | 704 |
| Arrival Heights | 5042 | 3122 | 258 |

* The Izaña NDACC coincidence data set is the only one in which TANSO-FTS measurements are more sparse. For consistency, Izaña was not treated as a special case.

coincidences is found in around 2 weeks. For ACE-FTS and the NDACC stations (combined), these coincidences occur over several months.

## 5 Averaging kernels

The averaging kernels of a profile retrieval provide information about the contributions of the retrieval from a priori information and the measurements. In this study, the retrieval methods for each data set differ, and the averaging kernel matrices are differently defined. In general, the rows of the averaging kernel matrix are peaked functions whose full width at half maximum (FWHM) can be used to define the vertical resolution of the measurement. The sum of the rows of the matrix gives the sensitivity, or response, of the retrieval. A sensitivity close to 1 indicates that most of the information in the retrieval comes from the measurement, while sensitivities less than 1 indicate increased reliance on the a priori in the solution.

The rows of the averaging kernel matrices for the ESA MIPAS, IMK-IAA MIPAS, TANSO-FTS, and the Eureka NDACC station are shown in Fig. 3. Each panel shows the mean from 30 retrievals. Vertical profiles of pressure associated with each retrieval's averaging kernel matrix are, in general, unique, so a common pressure grid was selected for each instrument, and averaging kernels were interpolated prior to averaging.

In this study, we treat TANSO-FTS retrievals as having the coarser vertical resolution in all cases, despite the widths of the kernel functions shown in Fig. 3a, which are comparable to MIPAS and narrower than NDACC. The peak locations of the TANSO-FTS averaging kernels do not match the corresponding pressure level of each kernel. Therefore the FWHM values when considering the location of the appropriate pressure level are much larger than the FWHM values for the averaging kernels of the other instruments.

In the NDACC retrievals, the a priori has a large role, and information coming from the measurements can hardly distinguish the contribution coming from the different altitudes. This leads to wide, overlapping averaging kernels. The IMK-IAA MIPAS retrievals use a form of Tikhonov regularization without an a priori. The ESA MIPAS retrievals use the regularizing Levenberg–Marquardt approach (where the parameter setting has been chosen to leave results largely independent from the initial-guess profiles) and a posteriori Tikhonov regularization without an a priori. The ACE-FTS retrievals do not use a regularized matrix inverse method. Consequently, the ACE-FTS and IMK-IAA MIPAS averaging kernels are very narrow, their peak values are close to 1 at each altitude where a spectrum was acquired, and the solutions do not rely on a priori information. Very similar averaging kernel are obtained also for ESA MIPAS, with wider widths at lower altitudes where the retrieval grid used is coarser than the measurement grid. The sensitivity of both ACE-FTS and MIPAS, shown in Fig. 3e, is close to 1 at all altitudes, falling off above 60 or 70 km. ACE-FTS averaging kernels are under development, and preliminary work is shown in Sheese et al. (2016).

The typical sensitivity of an NDACC retrieval is close to unity until above 20 km, falling off towards 0 through 60 km. The sensitivity of TANSO-FTS only reaches 0.2–0.3 between 5 and 10 km. The implication of such low values for sensitivity is that the TANSO-FTS retrievals are highly dependant on their a priori.

The trace of the averaging kernel matrix gives the DOFS. For example, DOFS for retrievals made by TANSO-FTS, IMK-IAA MIPAS, ESA MIPAS, and NDACC from observations over the Arctic, above 60° N, are shown in Fig. 4. The IMK-IAA MIPAS and TANSO-FTS data are in coincidence with one another. The NDACC data come from Eureka, Ny Ålesund, and Thule. The NDACC and ESA MIPAS data shown are the TANSO-FTS one-to-one coincidences used throughout this study (but are not coincident with the TANSO-FTS data shown in the top panel of Fig. 4). The trends visible are seasonal and are related to opacity and water vapour content. Recreating this figure over mid-latitudes or the tropics reveals a flat trend over time, while over Antarctica the trends are reversed in DOFS space.

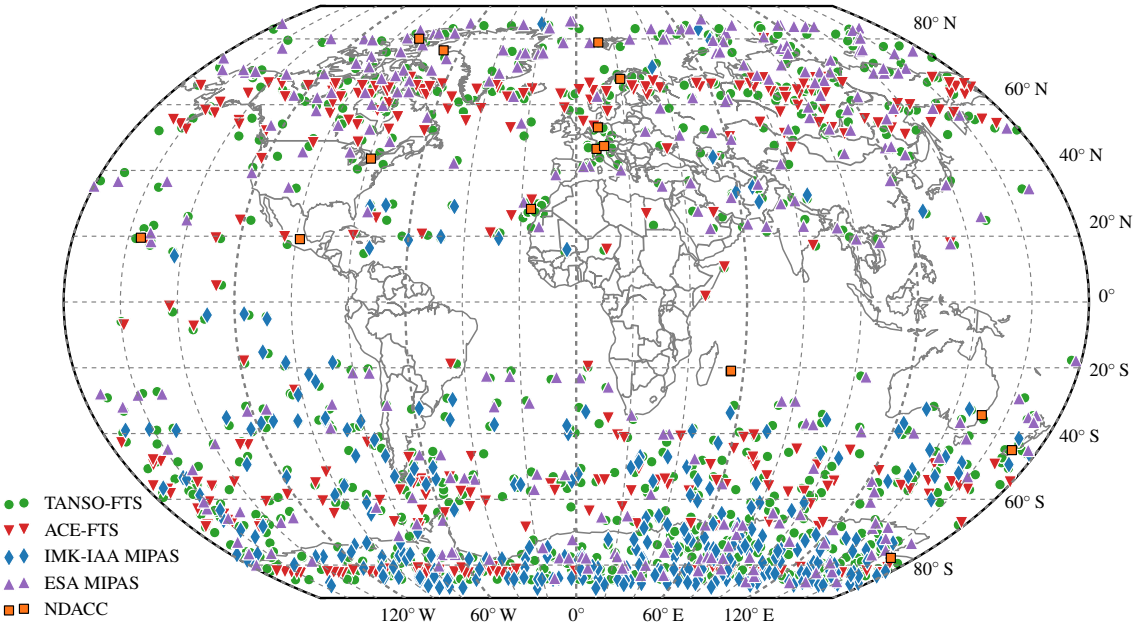


**Figure 2.** Locations of the first 200 observations of 2012 used in this study for TANSO-FTS (green), ACE-FTS (red), IMK-IAA MIPAS (blue), and ESA MIPAS (purple). The NDACC stations are shown in orange.

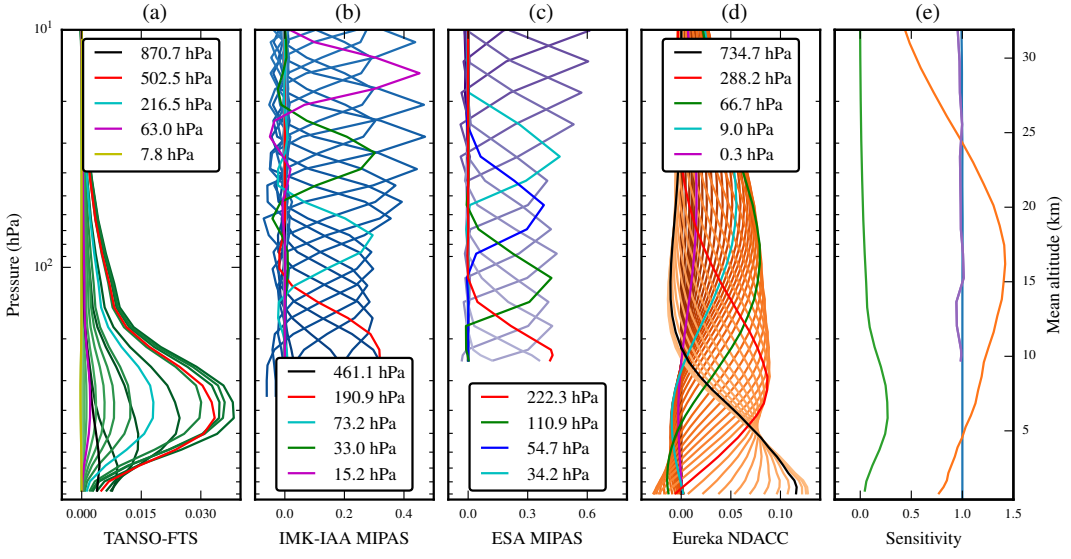


**Figure 3.** Example of averaging kernels for **(a)** TANSO-FTS, **(b)** IMK-IAA MIPAS, **(c)** ESA MIPAS, and **(d)** NDACC. Each kernel shown is the mean from 30 averaging kernel matrices from measurements made over the Arctic, interpolated to a common pressure grid. Panel **(d)** shows the mean averaging kernels from the Eureka station. Panel **(e)** shows the sensitivity for the mean averaging kernels shown in each panel: TANSO-FTS (green), IMK-IAA MIPAS (blue), ESA MIPAS (purple), and NDACC (orange).

The mean of the DOFS for the three NDACC stations over the Arctic is 1.98 with a standard deviation, $\sigma$, of 0.50. Over the tropics, considering data from Izaña, Réunion St. Denis, Altzomoni, and Mauna Loa (Réunion Maïdo only has data from 2013 onward, not shown here), the mean is 2.39 with $\sigma = 0.37$. The mean DOFS for IMK-IAA MIPAS are slightly larger than those for ESA MIPAS. Over the Arctic, their means and standard deviations are 17.05 and $\sigma = 1.06$ for IMK-IAA, and 15.76 and $\sigma = 0.93$ for and ESA, respectively. Over the tropics, they are 16.10 and $\sigma = 0.33$, and 15.88 and $\sigma = 1.20$.

The TANSO-FTS DOFS are larger at low latitudes, with a mean over the tropics of 0.72 and $\sigma = 0.08$, and means over the Arctic and Antarctic of 0.32 and 0.20, respectively

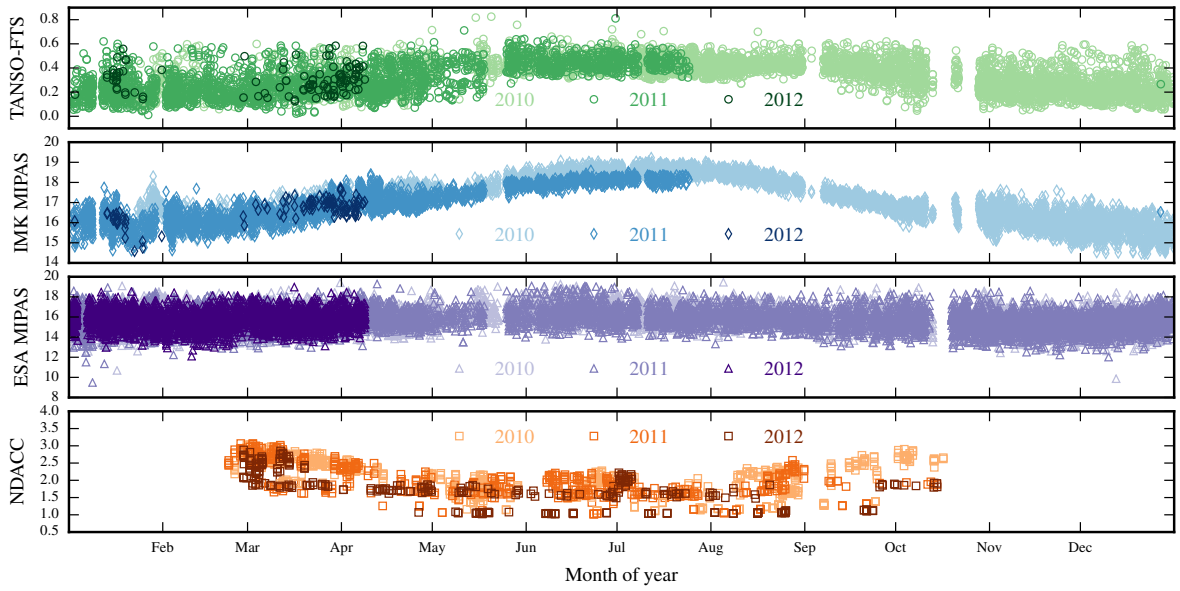


**Figure 4.** Degrees of freedom for signal for, from top to bottom, TANSO-FTS, IMK-IAA MIPAS, ESA MIPAS, and NDACC. Each satellite (and panel) uses a different symbol and colour, but the colour shades indicate the year the measurement was made in. The TANSO-FTS and IMK-IAA MIPAS measurements shown are in coincidence. The ESA MIPAS and NDACC data are from our analyzed data set but not in coincidence with the TANSO-FTS data in the top panel. All data are from the Arctic, 90–60° N, with the NDACC measurements from Eureka, Ny Ålesund, and Thule.

($\sigma = 0.13$ and 0.12). The DOFS for a TANSO-FTS retrieval rarely go above unity. Conversely, in the coincident NDACC data discussed above, over the tropics and Arctic, the DOFS never fall below unity. Note that the averaging kernel matrices for TANSO-FTS, and therefore the DOFS, cover a much smaller altitude range than for NDACC and MIPAS, which can extend above 100 km.

## 6 VMR vertical profile comparisons

### 6.1 Methodology

Retrievals made by an instrument with fine vertical resolution may result in structure over its vertical range that is not distinguishable in retrievals made by an instrument with coarser vertical resolution. In order to make the best comparison between two instruments with differing vertical resolution, it is necessary to smooth the vertical profiles retrieved from the finer-resolution instrument, in order to simulate what we could infer from it if it had a sensitivity similar to that of the other instrument. Smoothing is done using the a priori $CH_4$ VMR vertical profiles and averaging kernel matrices of the instrument with lower vertical resolution (Rodgers and Connor, 2003):

$$\hat{\boldsymbol{x}}_s = \boldsymbol{x}_a + \mathbf{A}(\hat{\boldsymbol{x}} - \boldsymbol{x}_a), \quad (1)$$

where $\hat{\boldsymbol{x}}$ is original higher-resolution retrieved profile, $\hat{\boldsymbol{x}}_s$ is the smoothed profile, $\boldsymbol{x}_a$ is the a priori profile of the lower-resolution retrieval, and $\mathbf{A}$ is the averaging kernel matrix of the lower-resolution retrieval. $\boldsymbol{x}_a$ and $\mathbf{A}$ are from the TANSO-FTS retrieval in all cases presented here. The smoothed profile, $\hat{\boldsymbol{x}}_s$, approximates the a priori, $\boldsymbol{x}_a$, when either the rows of $\mathbf{A}$ are close to 0, or when the retrieval is close to $\boldsymbol{x}_a$. As can be inferred from Fig. 3a, above 20–25 km $\hat{\boldsymbol{x}}_s \sim \boldsymbol{x}_a$.

In order to apply Eq. (1), all the variables on the right-hand side must be interpolated to a common grid. TANSO-FTS retrievals are done on a retrieved pressure grid. Determining the altitude of its VMR vertical profiles requires applying the equation of hydrostatic equilibrium and incorporating a priori temperature and water vapour. Since pressure is retrieved by ACE-FTS and MIPAS, and the tropospheric a priori pressure profiles and measured surface pressure are accurate for NDACC (Sepúlveda et al., 2014), all comparisons here have been done on a common pressure grid, as opposed to an altitude grid.

The data products do not always overlap over the entire pressure range of the common grid. Extrapolation is needed to ensure that the length of $\hat{\boldsymbol{x}}$ matches the dimensions of $\mathbf{A}$ in Eq. (1). For ACE-FTS and MIPAS, we use $\boldsymbol{x}_a$ to extend their retrieved profiles below their altitude range to cover the full pressure range of the TANSO-FTS averaging kernels. The averaging kernels at these non-overlapping pressure levels do not contribute to the smoothed retrieval at higher, overlapping levels. The following steps are taken to compute vertical profiles of the mean $CH_4$ VMR differences:

1. appropriate instrument data quality flags are applied to each VMR vertical profile in the coincidence pair;

2. TANSO-FTS a priori and validation target VMR vertical profiles are interpolated to the TANSO-FTS retrieval pressure grid;

3. the interpolated validation target profile is extended as needed to match the TANSO-FTS pressure range (and vector length) using the TANSO-FTS a priori;

4. the interpolated validation target profile is smoothed using the TANSO-FTS averaging kernel matrix using Eq. (1);

5. TANSO-FTS-retrieved and validation-target-smoothed VMR vertical profiles are interpolated to a standard pressure grid, and levels outside the pressure range of the target's VMR profile are discarded;

6. the piecewise difference between the TANSO-FTS and the smoothed validation target VMR vertical profiles is found;

7. the means, standard deviations, and correlation coefficients of the VMR differences are calculated at each level of the standard pressure grid for all coincidences within a latitude zone.

For comparison, mean VMR vertical profile differences were also computed without smoothing by using only steps 1, 5, 6, and 7. Zonally averaged VMR difference profiles are presented in Sect. 6.2, and results obtained without applying smoothing to the validation targets are shown in Sect. 6.3. The data quality flags in step 1, referring to variables in the data product files, were, for TANSO-FTS, CH4ProfileQualityFlag must be 0; for ACE-FTS, quality_flag must be 0 and cannot be equal to 4, 5, or 6 at any altitude; for ESA MIPAS, ch4_vmr_validity must be 1, and pressure_error cannot be NaN (not a number); and for IMK MIPAS, visibility must be 1, and akm_diagonal must be greater than 0.03.

Holl et al. (2016) found that identifying and removing coincident $CH_4$ VMR vertical profile pairs that may have one or both profile locations within a polar vortex, and then filtering these events, had little effect on their vertical profile comparisons below 25 km. Polar vortex event will have a much smaller effect on this study since it uses global and year-round data sets. For these two reasons, our method does not filter for profiles located within a polar vortex. Arrival Heights may be differently affected by a much stronger Antarctic polar vortex, but comparison results from this site are not anomalous and only account for 1.5 % of the NDACC data set, so they are treated in a consistent manner.

### 6.2 Zonally averaged VMR profile differences

Following Holl et al. (2016), we are trying to determine whether there are any zonal biases in the TANSO-FTS data or zonal dependencies when making comparisons to other instruments. The mean $CH_4$ VMR differences, averaged zonally, between the TANSO-FTS vertical profiles and the smoothed vertical profiles from ACE-FTS, IMK-IAA MIPAS, ESA MIPAS, and each NDACC station are show in Fig. 5. Each row in Fig. 5 shows the results from five latitudinal zones: 90–60° N, 60–30° N, 30° N–30° S, 30–60° S, and 60–90° S. The left-most column shows the mean differences between the retrievals from TANSO-FTS and those from the other instruments, always calculated as TANSO-FTS minus target. One standard deviation is shown for each instrument comparison with dotted lines. The middle-left column shows the mean differences as a percentage of the mean $CH_4$ VMR vertical profile taken for the target validation instrument in each zone. The number of VMR measurements used in the mean at each altitude, for each comparison, is shown in the right-most panel, with ESA MIPAS always having the most. At each altitude, we also calculated the Pearson correlation coefficient between the set of TANSO-FTS $CH_4$ VMR measurements and the coincident set from each validation instrument. These are shown in the middle-right column for each panel in Fig. 5.

For each zone, the mean difference tends towards 0, and the standard deviation falls off above 100 hPa. This is a reflection of the TANSO-FTS sensitivity. Above this altitude, the TANSO-FTS averaging kernels tend to 0, as shown in Fig. 3, and the smoothed profiles from each target instrument begin to approximate the TANSO-FTS a priori. Likewise, the TANSO-FTS retrieval above this pressure level is also close to its a priori. Conversely, the number of $CH_4$ VMR measurements in the mean falls off sharply below 10–12 km, or around 80–90 hPa, for the comparisons to the satellite instruments. For the satellite instruments and many of the NDACC stations we see the same trend: a positive bias (TANSO-FTS VMRs are greater than those of the validation instruments) decreasing with increasing altitude, with a tropospheric mean of around 20 ppbv, or 1 %. The bias is smallest for the two MIPAS data products in the tropics, between 30° N and 30° S. The bias relative to ACE-FTS is consistent in all the zones. For three of the NDACC stations – Ny Ålesund, Bremen, and Toronto – there is a negative bias (TANSO-FTS retrieves less $CH_4$ than these stations), and for Eureka and Jungfraujoch the bias is close to 0.

There is a notable feature just below 100 hPa in all the zones except 30–60° S. This feature is a pronounced increase in the mean difference in the northern zones 60–30° N and 90–60° N, while it is a decrease in the mean difference between 30° N and 30° S and between 60 and 90° S. It is around this pressure level, or altitude, that the VMR of $CH_4$ begins to fall off rapidly from between 1.8 and 2 ppmv in the troposphere towards 0 ppmv in the upper stratosphere and mesosphere. This feature indicates that the altitude at which this VMR decrease occurs differs between instruments. In the Northern Hemisphere this decrease in $CH_4$ VMR occurs at higher altitudes for TANSO-FTS than for the other instruments, and in the tropics and Southern Hemisphere

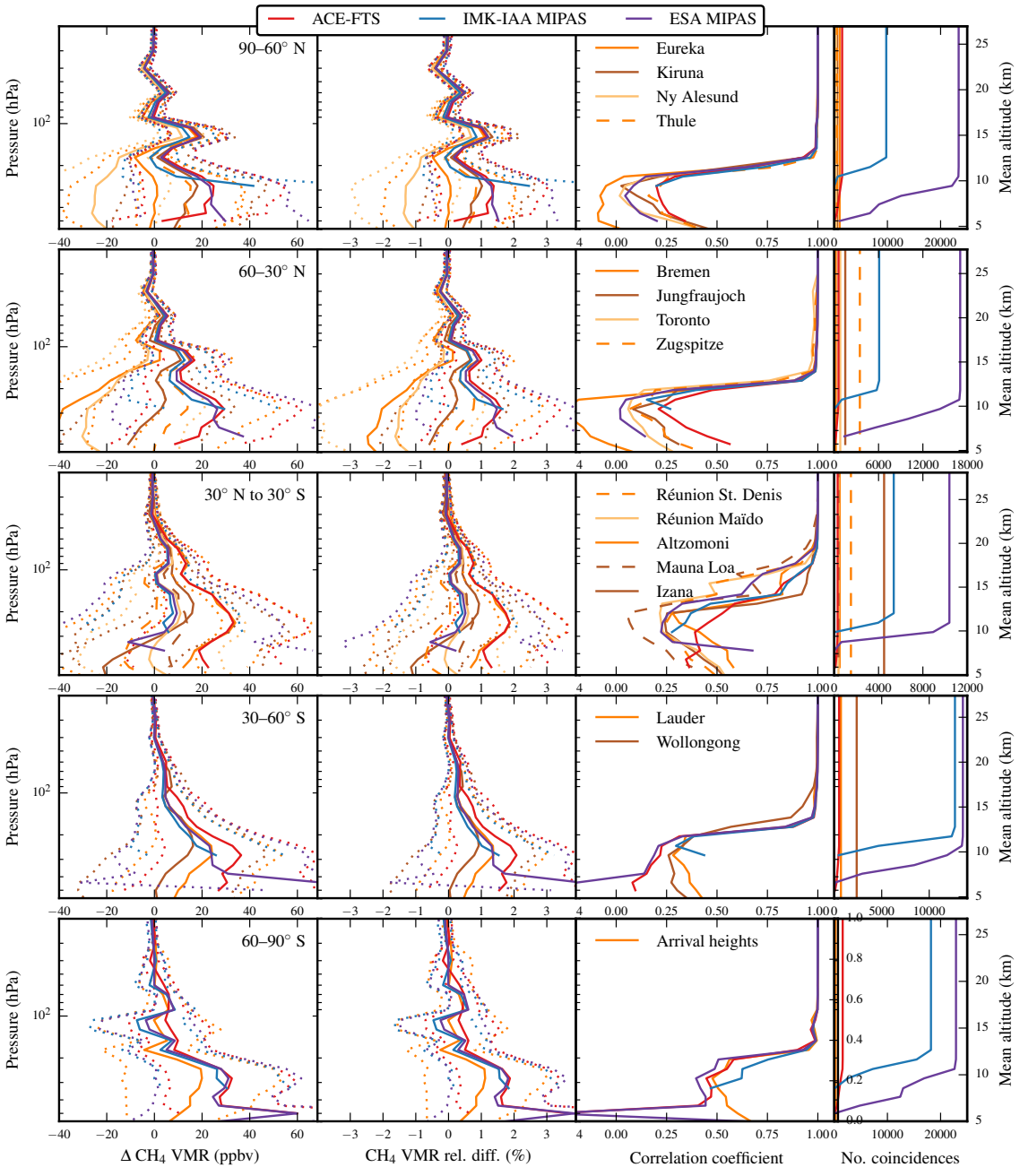


**Figure 5.** Zonally averaged comparison results. The rows present results for each zone, from top to bottom: 90–60° N, 60–30° N, 30° N–30° S, 30–60° S, and 60–90° S. In each row, the four panels show, from left to right, the mean $CH_4$ VMR difference between retrievals from TANSO-FTS and the validation target at each pressure level; the mean $CH_4$ VMR differences relative to the mean $CH_4$ VMR vertical profile of the validation target; the correlation coefficients $R^2$ of the $CH_4$ VMR differences for each coincident pair at each pressure level; and the number of coincidences at each pressure level. Differences are calculated as TANSO-FTS minus target for each data set compared. In all frames, ACE-FTS is shown in red, ESA MIPAS is purple, IMK-IAA MIPAS is blue, and NDACC stations are shades of orange. Each individual NDACC station with a zone is shown, and their shades indicated.

this decrease occurs more rapidly and at lower altitudes for TANSO-FTS.

For all instruments and in all zones, the correlation coefficients, $R^2$, at each altitude fall off very sharply, to around 0.2, below the 90 hPa level (and remain higher in the tropics). This indicates that biases seen in the mean differences are not uniform across the coincident data set and that there is significant variability in the magnitudes of the differences

for individual vertical profile pairs and in the direction of the difference. This is related not only to the increasing standard deviation of the differences with decreasing altitude but also to the standard deviations of each data product in the comparison. The sharpness and altitude of the decrease are directly related to the TANSO-FTS averaging kernels. Above the 100 hPa level, the standard deviations of the TANSO-FTS and the smoothed validation target fall off very sharply as they both begin to approximate the a priori (which also explains why $R^2$ is close to 1).

### 6.3 Impact of smoothing

This study was also performed without applying any smoothing to the vertical profiles of the target validation instruments. These results are shown in Fig. 6, which has the same panels as Fig. 5. The data have not been separated zonally, and the plots show means for all latitudes. No zonal biases were observed in the unsmoothed data. The 16 NDACC stations have been combined into a single data set.

Figure 6 shows the mean differences between the TANSO-FTS data product and those of other instruments, and the behaviour of the comparisons at higher altitudes when the validation targets are unaffected by the TANSO-FTS averaging kernels. Without the smoothing applied, the difference profiles in Fig. 6 show more consistent behaviour over the pressure, or altitude, range shown. While the magnitude of the differences is much greater without smoothing, it is not consistently biased high or low for all the data products at all altitudes. When comparing to the satellite instruments in the upper troposphere, we find that the TANSO-FTS retrieval has greater $CH_4$ VMRs by around 50 ppbv, or around 3 %.

For context, a comparison between the ACE-FTS and ESA MIPAS data products, using profiles that were coincident with the same TANSO-FTS observation, is shown in grey. The mean differences between these two data products are smaller than those relative to TANSO-FTS but have comparable standard deviations and a slightly smaller correlation, with $R^2 = 0.5$ and 0.6 in the upper troposphere.

The comparison between TANSO-FTS and NDACC extends below the range of ACE-FTS and MIPAS. NDACC and TANSO-FTS agree very well in this region, between $\pm 30$ ppbv, or between $\pm 2$ %. In this case, the NDACC stations retrieve more $CH_4$, on average. The low-altitude NDACC and TANSO-FTS data are also more closely linearly correlated, between 50 and 60 %. It should also be noted that the standard deviation of the TANSO-FTS and NDACC differences is also less than those for ACE-FTS and MIPAS at all altitudes.

## 7 Partial column comparisons

### 7.1 Methodology

For each $CH_4$ VMR vertical profile in a pair of coincident measurements, we computed a partial column and compared those from TANSO-FTS to each of the other instruments to investigate how well correlated the derived $CH_4$ abundances are. For consistency, each pair of partial columns must be calculated over the same pressure range, as the number of molecules in the column strongly depends on the altitude range (length of the column) of the integral. To determine the pressure range over which to compute partial columns for each coincident pair of profiles, we considered the TANSO-FTS averaging kernels.

We investigated the sensitivity of the TANSO-FTS retrievals, as defined in Sect. 5 to find an altitude range which minimizes the partial column dependence on a priori information, ensuring our investigation is focused on retrieved information from TANSO-FTS. Figure 7 shows a two-dimensional histogram of the number of TANSO-FTS profiles, for all validation targets combined for two criteria: setting a requirement that the sensitivity must be greater than some threshold and the resulting number of usable pressure levels in the integral for each profile. We see that the maximum number of usable levels falls off in an approximately linear manner with increasing sensitivity threshold, and that for any sensitivity threshold there will be a large number of TANSO-FTS $CH_4$ VMR vertical profiles that never meet the sensitivity criteria. Increasing the sensitivity cutoff by 0.05 causes approximately 10 000 additional TANSO-FTS vertical profiles, or around 6 % of the total data set combining all validation targets, to fail to meet the requirement at any altitude. The number of usable pressure levels given a restriction on sensitivity is not normally distributed, as can be inferred from the empty area in the upper right of Fig. 7.

For this study, we have selected a sensitivity threshold of 0.2 and require a minimum of three integrable pressure levels. Approximately 23 % of the TANSO-FTS retrievals do not meet these criteria. In such a case, partial columns are still computed using three pressure levels surrounding the level with the maximum sensitivity that are within the range of the target profile (e.g., not below 10 km when comparing to ACE-FTS). These excluded data do not exhibit a broader distribution, but their computed partial columns are all very small due to the integration range. Because the overlapping altitude regions for NDACC and TANSO-FTS measurements extend much lower in the atmosphere than for ACE-FTS and MIPAS, the number of TANSO-FTS profiles that do not meet the sensitivity criteria is much smaller for NDACC.

Partial columns are computed as

$$\text{column} = \int_{z_1}^{z_2} \frac{P(z)}{kT(z)} \chi(z) \mathrm{d}z, \tag{2}$$

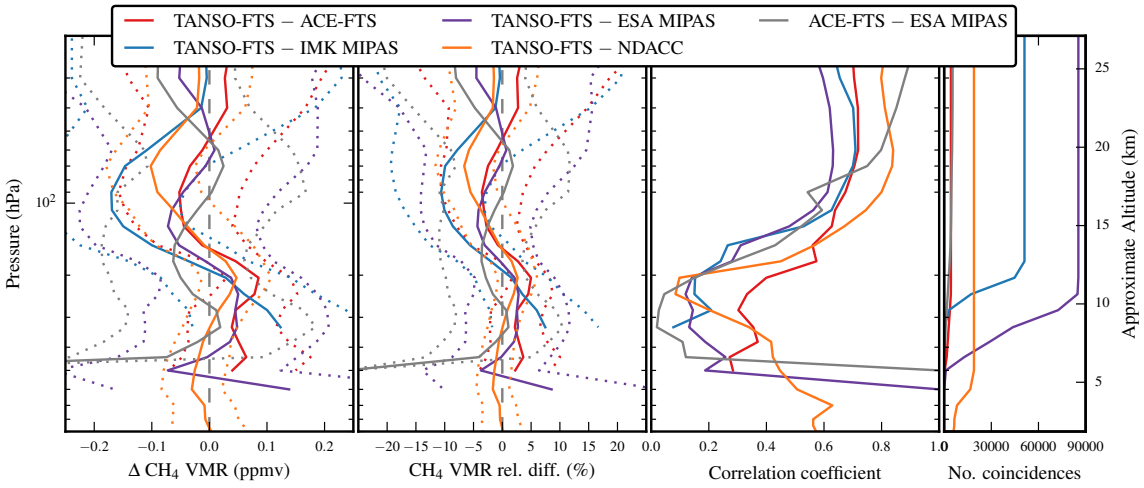


**Figure 6.** Averaged comparison results, as in each panel of Fig. 5, for all latitudes, without applying smoothing to the validation instruments' $CH_4$ VMR vertical profiles. Differences are calculated as TANSO-FTS minus target for each data set compared (and ACE-FTS-ESA MIPAS for that case).

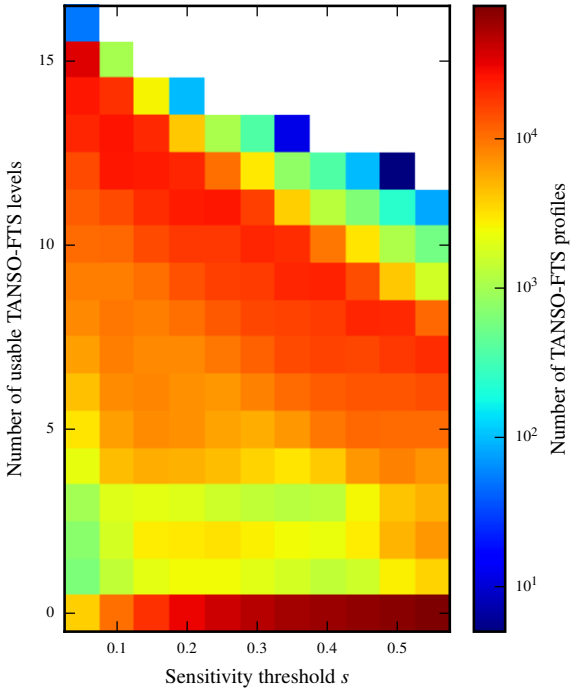


**Figure 7.** Two-dimensional histogram showing the number of TANSO-FTS $CH_4$ VMR profiles within our data set ($z$ axis) that have some number of usable pressure levels ($y$ axis) with a sensitivity greater than some given threshold, $s$ ($x$ axis). The data set shown here consists of all TANSO-FTS observations that are one-to-one coincident with a target validation data set. The threshold chosen for this study was $s = 0.2$.

where $z_1$ and $z_2$ bound the integration range over altitude $z$, $P$ is pressure, $T$ is temperature, $\chi$ is the $CH_4$ VMR, and $k$ is the Boltzmann constant. For each instrument, $\chi(z)$ is the retrieved quantity, and either retrievals were performed on a pressure grid or pressure was retrieved simultaneously. We compute partial columns from vertical profiles after step 5 in Sect. 6.1, so both the TANSO-FTS and the smoothed validation target profiles have the same pressure at each level in the integration. Since TANSO-FTS retrievals do not have an altitude grid, we use that of the coincident measurement, which corresponds to the pressure levels and should be very accurate within the altitude range considered in this study (upper troposphere to lower stratosphere). Thus, we are integrating over the same altitude range for both instruments. Since ACE-FTS and both MIPAS data products include retrieved temperatures, we use their retrieved temperature. For TANSO-FTS and NDACC, we use their corresponding a priori temperatures.

Several methods of integration were investigated, and the results presented in Sect. 7.2 are derived by simple summation of the integrand multiplied by the bin width of each data point in kilometers. We also used numerical integration techniques, variations of Newton–Cotes and Gaussian quadrature formulas. These did not provide significantly different results due the large size of our sample (i.e., our results are statistics found from the least-squares method, and small differences in the individual partial columns due to different integration methods do not introduce bias). Since the analytic function being integrated is not well defined, neither is the uncertainty of the derived partial column. Propagating reported retrieval uncertainties of temperature and VMR provides the most appropriate estimate of uncertainty, which is shown in Fig. 8.

### 7.2 Partial column correlation

The computed partial columns from TANSO-FTS are plotted against those from each validation instrument in Fig. 8. The

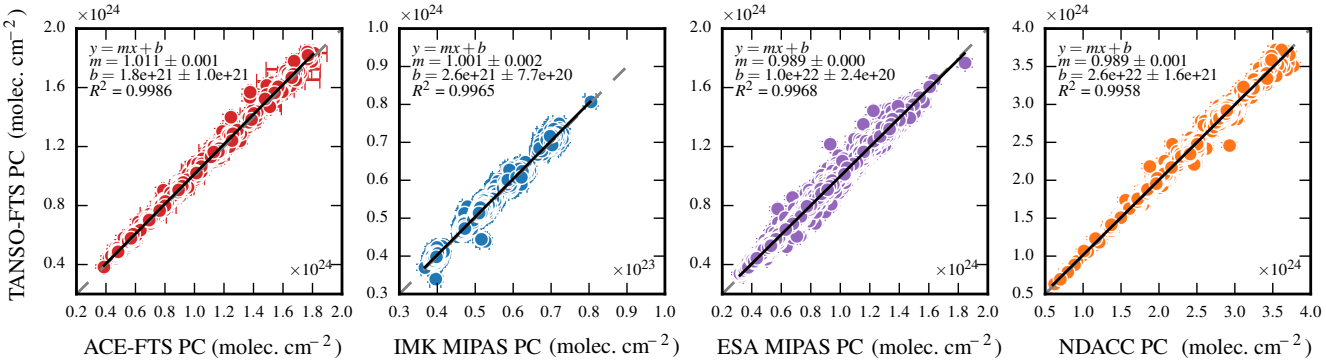


**Figure 8.** Partial column (PC) correlation plots comparing TANSO-FTS $CH_4$ to each validation instrument. Comparisons to ACE-FTS are red, to IMK-IAA MIPAS are blue, to ESA MIPAS are purple, and to NDACC are orange. The vertical range of partial column integration varies for each pair of coincident profiles based on the criteria described in Sect. 7.1. The statistics for weighted linear least-squares regression are shown, with weights equal to $1/(\delta_x^2 + \delta_y^2)$.

panels for ACE-FTS, ESA MIPAS, and IMK-IAA MIPAS contain measurements for all latitudes, and that for NDACC combines results from all 16 stations. Since IMK-IAA retrievals do not extend as low as those of ESA generally, the altitude range of the partial column integral is often smaller than those of the other instruments, resulting in smaller $CH_4$ abundances. Conversely, abundances when comparing to the NDACC stations are the largest.

The Pearson correlation coefficients, $R^2$, are 0.9986, 0.9965, 0.9968, and 0.9958 for ACE-FTS, IMK-IAA MIPAS, ESA MIPAS, and NDACC, respectively. The slopes of the fitted correlation lines are all close to unity, and a small bias is seen in the $y$ intercept corresponding to between 0.4 and 2.8 % relative to the mean partial columns of the validation targets, with the greatest corresponding to the NDACC data. Among the individual NDACC stations, those with the largest correlation function intercept are Mauna Loa, Jungfraujoch, Bremen, Izaña, and Zugspitze ($1.2 \times 10^{23}$–$7.5 \times 10^{23}$). TANSO-FTS has a negative intercept only with respect to two stations: the correlation coefficients for each station are all greater than 0.96, except for Mauna Loa, Izaña, and Réunion Maïdo, which all happen to be islands and for which a large number of coincident TANSO-FTS measurements would have been made over water (see Sect. 8).

Statistics regarding the distribution of the integration ranges over altitude are given in Table 3. This table gives the number of coincident pairs for each validation instrument for which the TANSO-FTS $CH_4$ VMR vertical profile passed the sensitivity requirements. It also gives the mean and standard deviation of the lower bound of the integral (lower altitude), the width of the interval (highest altitude minus the lowest altitude), and the number of pressure levels used. As expected, the NDACC stations have the widest altitude range, while the IMK-IAA MIPAS retrievals have the smallest. Note that the column in Table 3 showing number of levels used does not correspond to the mode in Fig. 7 since Fig. 7 considers only the TANSO-FTS averaging kernels and does not reflect the lack of available comparison data at lower altitudes.

Repeating the analysis using unsmoothed data from ACE-FTS, ESA and IMK-IAA MIPAS, and NDACC, the spread in the correlation plots increases and the biases observed in the intercepts increase, while the correlation coefficients remain very close to unity. Figure 9 shows derived partial column correlation plots for each validation target instrument. The intercept without smoothing is between 2 and 6 %. The correlation coefficient for the MIPAS instruments is reduced to 0.97.

## 8 Discussion

The objective of this study was to quantitatively assess TANSO-FTS $CH_4$ VMR vertical profile retrievals compared with other FTS instruments and to further investigate whether there were any biases with latitude or other retrieval parameters. As shown in Sect. 6.2, we did not find a significant difference in mean $CH_4$ VMR profile differences between latitudinal zones.

To investigate further, we consider the $CH_4$ VMR differences averaged over altitude for each coincident pair, for each validation instrument. To choose the altitude range over which to find the mean, we use the same sensitivity criteria developed in Sect. 7.2. The resulting mean differences between TANSO-FTS and ACE-FTS, MIPAS, and NDACC are shown as a function of latitude in Fig. 10. Weighted least-squares regression of the combined data sets for each hemisphere reveals a bias at all latitudes of 13.30 ± 0.06 ppbv. There is also a small slope in the data from each hemisphere, decreasing from the poles to the tropics. Linear fit parameters for the combined data sets in each hemisphere are given in Table 4. This leads to a bias of around 4 ppbv in the tropics (0.25 % of a tropical tropospheric VMR value of 1.8–2 ppmv) and of 0.014 and 0.020 ppmv at the North and South

**Table 3.** Statistics for the partial column integration ranges for ESA MIPAS, IMK-IAA MIPAS, ACE-FTS, and NDACC stations with the requirements that the TANSO-FTS sensitivity, $s$, is greater than 0.2 for at least three pressure levels. The number of coincident profiles passing this criterion, $N$, and its percentage of one-to-one coincidences found in this study are given. Means and standard deviations are given for the minimum altitudes, min($z$); total integration range, $z_{\text{range}}$; and number of levels used, $n$.

| Target | Profiles with $s > 0.2$ | | Lowest altitude (km) | | Altitude range (km) | | Number of levels | |
|---|---|---|---|---|---|---|---|---|
| Instrument | $N$ | (%) | min($z$) | $\sigma_{\min(z)}$ | $z_{\text{range}}$ | $\sigma_{z_{\text{range}}}$ | $n$ | $\sigma_n$ |
| ESA MIPAS | 52 016 | 60.9 | 8.4 | 1.5 | 4.6 | 1.5 | 4.8 | 1.1 |
| IMK-IAA MIPAS | 17 787 | 34.8 | 11.3 | 0.6 | 3.5 | 0.9 | 3.7 | 0.6 |
| ACE-FTS | 2562 | 59.6 | 7.3 | 1.4 | 5.2 | 2.3 | 5.4 | 1.8 |
| Total NDACC | 18 587 | 98.0 | 3.3 | 1.0 | 11.3 | 2.1 | 10.4 | 1.5 |

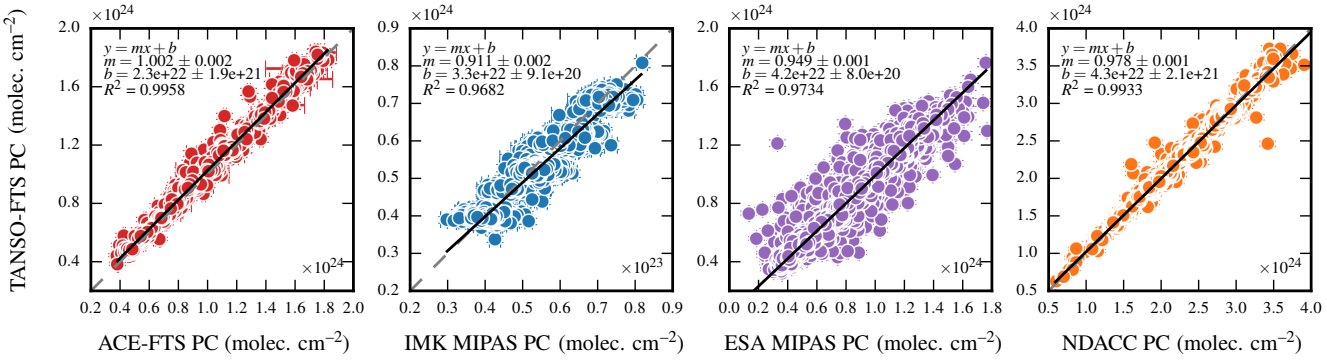


**Figure 9.** As in Fig. 8 but for partial column correlation results using unsmoothed $CH_4$ VMR vertical profiles for each validation instrument.

**Table 4.** Least-squares regression statistics for the data in each hemisphere plotted in Fig. 10. Results from all four validation target data sets are combined.

| | Slope (ppbv/° latitude) | Intercept (ppbv) | $R^2$ |
|---|---|---|---|
| Northern | $0.113 \pm 0.005$ | $5.3 \pm 0.3$ | 0.08 |
| Southern | $-0.207 \pm 0.004$ | $3.1 \pm 0.2$ | 0.18 |

Pole, respectively (or around 1 %). The biases are latitude-dependent and vary between the tropics and the poles.

We also compared the differences shown in Fig. 10 to TANSO-FTS retrieval parameters: land or sea mask, sunglint flag, incident angle along the scan path, incident angle along the GOSAT track path, and observation mode (see Kuze et al., 2009). Each parameter was compared to the latitudes and the mean differences in Fig. 10, and the regression and covariance statistics from least-squares fitting were computed. We found no biases in our coincident TANSO-FTS data set related to any of these parameters or whether the observation was made during night or day. The land or sea mask is an indicator of whether the retrieval was made over land, water, or a combination in the field of view. In our data set of all one-to-one coincidences between TANSO-FTS and the validation targets, 54.0 % of TANSO-FTS measurements were made over water, 36.3 % were made over land, and 9.6 % were a mixture. The sunglint flag indicates whether the positions of the sun, satellite, and observation point are related within a predefined range, qualifying the observation as being made in sunglint mode. In our data set, only 1.6 % of TANSO-FTS measurements are sunglint observations, and they are all over water and within ±45° latitude. Finally, 54.1 % of TIR observations were made at night.

The primary driver of the mean differences found when comparing TANSO-FTS to other FTS instruments, with and without smoothing, is the instrument design and observation geometry. TANSO-FTS is a much more compact and, therefore, coarser-spectral-resolution FTS than those used in the comparison. The coarser spectral resolution makes it harder to distinguish closely spaced absorption lines, leading to poorer vertical sensitivity and higher uncertainty in the measurements. While the TIR spectral range of TANSO-FTS is comparable to that of MIPAS, the mid-infrared ranges of NDACC and ACE-FTS include a very strong methane absorption band near 3000 cm$^{-1}$ with little interference from $CO_2$, increasing their sensitivity and ability to accurately constrain $CH_4$ retrievals. Furthermore, MIPAS and ACE-FTS observe the limb of the atmosphere, providing them with more measurements per retrieved profile, improved vertical resolution, and much higher sensitivity. While NDACC instruments also only have a single spectrum per retrieved profile, they observe the sun directly (as does ACE-FTS), re-

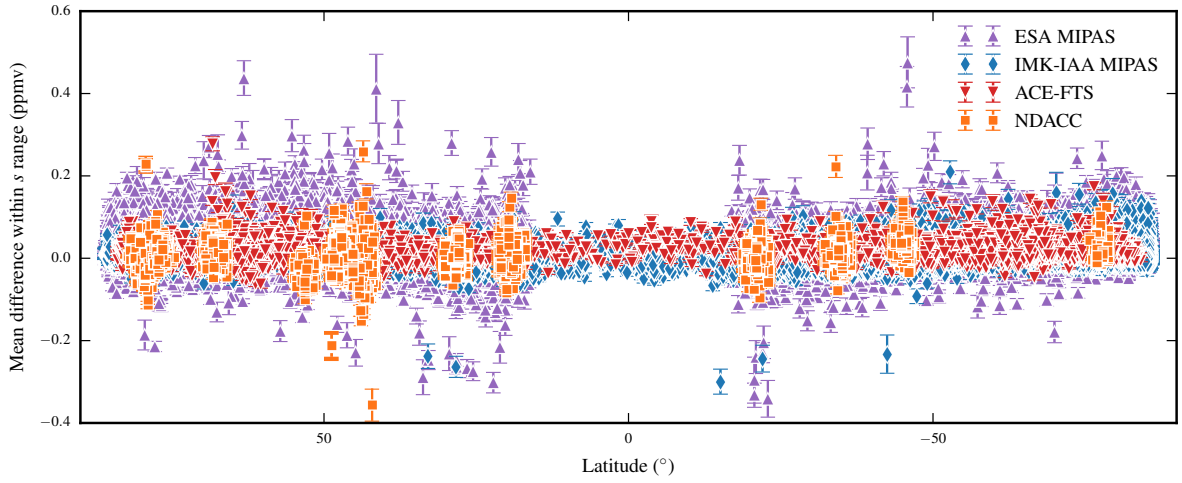


**Figure 10.** Mean $CH_4$ VMR differences between TANSO-FTS and each validation target data set, averaged vertically using the altitude range selected for integrating partial columns as a function of latitude. Differences are calculated as TANSO-FTS minus target for each data set compared.

sulting in a very strong signal. All these factors contribute to TANSO-FTS performing retrievals on a lower-spectral-resolution measurement of a weaker signal compared to MIPAS, ACE-FTS, and the NDACC sites. This results in the sensitivity and DOFS shown in Figs. 3 and 4.

In Sect. 3, we examined the variability within each data set. This gives an idea of some of the sources of error in our comparison. The coincidence criteria used allow for the comparison of retrieved $CH_4$ vertical profiles from different air masses. Our investigation of the NDACC data provides an estimate of the dependence of the $CH_4$ abundance on time, since we compared profiles retrieved from the same location using the same retrieval algorithms but at different times of day. Our result shows that temporal spacing may contribute around 5 ppbv. Our investigation of the ACE-FTS variability fixed the instrument and retrieval algorithm but compared observations of different air masses, and we found a similar result of only several ppbv. The largest variability was exhibited when we investigated the MIPAS data set. This comparison was of the same observations analyzed by different retrieval algorithms (IMK-IAA and ESA) and resulted in much larger mean differences on the order of 100 ppbv.

Differences in retrieval algorithms between TANSO-FTS and the validation instruments may also account for the differences found in Figs. 5 and 6. Small differences in spectroscopic parameters exist; for example, each instrument's retrieval algorithms use different editions of the HITRAN line list. Comparisons of these line lists, and their impact on retrievals, can be found in, e.g., Boone et al. (2013), Rothman et al. (2013), and Toon et al. (2016). The most significant parameter for TANSO-FTS is its a priori due to the weight given to the a priori profile by the TANSO-FTS averaging kernels in the retrieval. In Sect. 3 we compared the TANSO-FTS-retrieved vertical profiles of $CH_4$ to the corresponding a priori profiles and found that they differ, on average, by up to 30 ppbv. This provides a rough minimum of the accuracy of the a priori profiles required for the retrievals.

## 9 Conclusions

The TANSO-FTS TIR $CH_4$ vertical profile data product is an important and novel data set. Its vertical range extends lower into the troposphere than other satellite data products, and its spatial coverage is global with a high density of measurements. We have investigated the sensitivity and averaging kernels for the TANSO-FTS data product and done a global comparison with four other FTS data products. Our comparisons showed that the sensitivity of the TANSO-FTS retrieval is relatively low at all altitudes and that there is a limitation on the upper altitude of its data product of around 15 or 20 km. Unfortunately, the lower-altitude boundaries of the other satellite-based data products, between 7 and 15 km, reduce the vertical range over which we can make comparisons. In the upper troposphere, we found good agreement between TANSO-FTS and NDACC, without a bias. The agreement between these two data sets persisted regardless of whether smoothing was applied to the NDACC data. Therefore, despite the lower sensitivity of the TANSO-FTS data product, it remains an important and unique data set of global tropospheric $CH_4$ measurements.

In the overlapping altitude ranges of the three satellite data products, we found a small, but consistent, positive bias of around 20 ppbv, or 1 %. We found that the shapes of the TANSO-FTS $CH_4$ VMR vertical profiles near 15 km, where the $CH_4$ VMR falls off with increasing altitude, does not match those of the other instruments, and in a consistent manner, resulting in a pronounced feature in the mean differ-

ence profiles in Fig. 5, just below the 100 hPa level. Despite the large variability in each data set and in the differences between the TANSO-FTS retrievals and the others, we found that partial columns computed from the vertical profiles were very tightly correlated, with and without smoothing.

When looking for a relationship between latitude and the differences between data products, we found a small, but statistically significant, dependence of the vertically averaged differences on latitude. The TANSO-FTS data product shows better agreement over the tropics than the poles.

We look forward to future versions of the retrieval which may feature a greater sensitivity and altitude range, while reducing the small biases and dependence on the a priori profiles. In a future release, the a priori will not be changed but remain the outputs of the NIES-TM. Kuze et al. (2016) used theoretical simulations to determine that the Level 1B spectra which were used (V161) to generate the current TIR $CH_4$ data product had considerable uncertainties. New Level 1B spectra are due for release in 2018 and should lead to improved retrievals. Kuze et al. (2016) also proposed some corrections to the TANSO-FTS TIR L1B spectra which may be implemented. The spectral line list used (HITRAN 2008) will be updated. Uncertainties in the surface emissivity over cold surfaces (snow and ice) affect the retrieval at higher altitudes and will be improved in the next release. Improvements are also being made to the way the retrieval handles and simultaneously retrieves interfering species, such as $O_3$.

*Data availability.* All data used in this study except for that from GOSAT TANSO-FTS are available upon request and accessed through appropriate Web portals. The ACE-FTS Science Team at the University of Waterloo provided access to their Level 2 data through https://databace.scisat.ca/level2/ (registration required). Access to the ESA MIPAS Level 2 data was granted and provided through the ESA Earth Online portal: https://earth.esa.int/ (registration required). The IMK-IAA MIPAS Level 2 data were accessed using the KIT website: https://www.imk-asf.kit.edu/english/308.php (registration required). NDACC data have been compiled by many independent research groups and were accessed through a National Centers for Environmental Prediction FTP server, with each station being accessible through https://www.ndsc.ncep.noaa.gov/data/data_tbl/. Early access to the TANSO-FTS TIR CH4 VMR vertical profiles was provided through the GOSAT User Interface Gateway: https://data.gosat.nies.go.jp/ (no longer functional). Regular access to the TANSO-FTS data products is available at https://data2.gosat.nies.go.jp/index_en.html (registration required).

*Author contributions.* The work presented here was done by KSO with input from and under the supervision of KS, KAW, and NS. KSO prepared the manuscript with contributions from all co-authors. $CH_4$ retrievals were developed and provided, with additional input, by NS for TANSO-FTS, CDB for ACE-FTS, PR for ESA MIPAS, JP for IMK-IAA MIPAS, MG for Altzomoni, JWH for Thule and Mauna Loa, FH for Kiruna, NJ for Wollongong, WB for Jungfraujoch, MdM for Réunion St. Denis and Maïdo, JN for Bremen and Ny Ålesund, MS for Izaña, DS for Lauder and Arrival Heights, SC and KS for Eureka and Toronto, and RS for Zugspitze.

*Competing interests.* The authors declare that they have no conflict of interest.

*Acknowledgements.* This research was conducted under the framework of the Japan Aerospace Exploration Agency (JAXA), National Institute for Environmental Studies (NIES), and the Ministry of the Environment (MOE) Research Announcement (RA) project "GOSAT Validation Using Eureka and Toronto Ground-Based Measurements and ACE, CloudSat, and CALIPSO Satellite Data", which was supported by the Canadian Space Agency (CSA), the Natural Sciences and Engineering Research Council of Canada (NSERC), and Environment & Climate Change Canada (ECCC). This work is the result of many long-lasting collaborations, and we would like to thank our co-authors and collaborators for providing data and expertise. The GOSAT team provided early access to its TANSO-FTS TIR $CH_4$ VMR vertical profiles through the GOSAT User Interface Gateway. SCISAT/ACE is a Canadian-led mission mainly supported by the CSA and NSERC. The ACE-FTS Science Team at the University of Waterloo provided access to their Level 2 data, as well as expert knowledge with its interpretation and quality management. Access to the ESA MIPAS Level 2 data was granted and provided through the ESA Earth Online portal. The IMK-IAA MIPAS Level 2 data were accessed using the KIT website. NDACC data have been compiled by many independent research groups and were accessed through a National Centers for Environmental Prediction FTP server. Measurements at PEARL were made by the Canadian Network for the Detection of Atmospheric Change (CANDAC), led by James R. Drummond, and in part by the Canadian Arctic ACE/OSIRIS Validation Campaigns, led by Kaley A. Walker. Support is provided by AIF/NSRIT, CFI, CFCAS, CSA, EC, GOC-IPY, NSERC, NSTP, OIT, PCSP, and ORF. Logistical and operational support is provided by PEARL Site Manager Pierre Fogal, CANDAC operators, and the ECCC weather station. Measurements at the University of Toronto Atmospheric Observatory were supported by CFCAS, ABB Bomem, CFI, CSA, EC, NSERC, ORDCF, PREA, and the University of Toronto. NDACC data analysis at Toronto and Eureka was supported by the CAFTON project, funded by the CSA's FAST Program. The National Institute of Water and Atmospheric Research Ltd (NIWA) ground-based FTSs are core-funded through New Zealand's Ministry of Business, Innovation and Employment. We thank Antarctica, New Zealand, and the Scott Base staff for providing logistical support at Arrival Heights. Measurements at the Jungfraujoch station are primarily supported by the Fonds de la Recherche Scientifique (F.R.S.–FNRS) and the Fédération Wallonie-Bruxelles, both in Brussels. The Swiss GAW-CH program of MeteoSwiss is further acknowledged. We thank the International Foundation High Altitude Research Stations Jungfraujoch and Gornergrat (HFSJG, Bern) for supporting the facilities needed to perform the observations and the many colleagues who contributed to FTS data acquisition at that site. Whitney Bader has received funding from the European Union's Horizon 2020 research and innovation program under the Marie Skłodowska-Curie actions grant agreement no. 704951. We would like to thank Alejandro Bezanilla,

who operates the Altzomoni site, and Wolfgang Stremme, who does the data processing for the Altzomoni site and uploads the data to the NDACC archive. Altzomoni is supported by Consejo Nacional de Ciencia y Tecnología (CONACYT, grants 239618 and 249374) and la Dirección General de Asuntos del Personal Académico de la Universidad Nacional Autónoma de México (DGAPA-UNAM, grants IN109914 and IA101814).

Edited by: Helen Worden
Reviewed by: two anonymous referees

## References

Bader, W., Bovy, B., Conway, S., Strong, K., Smale, D., Turner, A. J., Blumenstock, T., Boone, C., Collaud Coen, M., Coulon, A., Garcia, O., Griffith, D. W. T., Hase, F., Hausmann, P., Jones, N., Krummel, P., Murata, I., Morino, I., Nakajima, H., O'Doherty, S., Paton-Walsh, C., Robinson, J., Sandrin, R., Schneider, M., Servais, C., Sussmann, R., and Mahieu, E.: The recent increase of atmospheric methane from 10 years of ground-based NDACC FTIR observations since 2005, Atmos. Chem. Phys., 17, 2255–2277, https://doi.org/10.5194/acp-17-2255-2017, 2017.

Baray, J. L., Courcoux, Y., Keckhut, P., Portafaix, T., Tulet, P., Cammas, J. P., Hauchecorne, A., Godin, S., Beekmann, S., de Mazière, Hermans, C., Desmet, F., Sellegri, K., Colomb, A., Ramonet, M., Sciare, J., Vuillemin, C., Hoareau, C., Dionisi, D., Duflot, V., Vérèmes, H., Porteneuve, J., Gabarrot, F., Gaudo, T., Metzger, J.-M., Payen, G., Leclair de Bellevue, J., Barthe, C., Posny, F., Ricaud, P., Abchiche, A., and Delmas, R.: Maïdo observatory: a new high-altitude station facility at Reunion Island (21° S, 55° E) for long-term atmospheric remote sensing and in situ measurements, Atmos. Meas. Tech., 6, 2865–2877, https://doi.org/10.5194/amt-6-2865-2013, 2013.

Batchelor, R. L., Strong, K., Lindenmaier, R., Mittermeier, R. L., Fast, H., Drummond, J. R., and Fogal, P. F.: A new Bruker IFS 125HR FTIR spectrometer for the Polar Environment Atmospheric Research Laboratory at Eureka, Canada: measurements and comparison with the existing Bomem DA8 spectrometer, J. Atmos. Ocean. Tech., 26, 1328–1340, https://doi.org/10.1175/2009JTECHA1215.1, 2009.

Baylon, J. L., Stremme, W., Plaza, E., Bezanilla, A., Grutter, M., Hase, F., and Blumenstock, T.: $CO_2$ total column variability from ground-based FTIR measurements over central Mexico, in: AGU Fall Meeting, AGU Fall Meeting, 2014.

Bernath, P. F.: The Atmospheric Chemistry Experiment (ACE), J. Quant. Spectrosc. Ra., 186, 3–16, https://doi.org/10.1016/j.jqsrt.2016.04.006, 2017.

Bernath, P. F., McElroy, C. T., Abrams, M. C., Boone, C. D., Butler, M., Camy-Peyret, C., Carleer, M., Clerbaux, C., Coheur, P.-F., Colin, R., DeCola, P., de Mazière, M., Drummond, J. R., Dufour, D., Evans, W. F. J., Fast, H., Fussen, D., Gilbert, K., Jennings, D. E., Llewellyn, E. J., Lowe, R. P., Mahieu, E., McConnell, J. C., McHugh, M., McLeod, S. D., Michaud, R., Midwinter, C., Nassar, R., Nichitiu, F., Nowlan, C., Rinsland, C. P., Rochon, Y. J., Rowlands, N., Semeniuk, K., Simon, P., Skelton, R., Sloan, J. J., Soucy, M.-A., Strong, K., Tremblay, P., Turnbull, D., Walker, K. A., Walkty, I., Wardle, D. A., Wehrle, V., Zander, R., and Zou, J.: Atmospheric Chemistry Experiment (ACE): Mission overview, Geophys. Res. Lett., 32, L15S01, https://doi.org/10.1029/2005GL022386, 2005.

Blumenstock, T., Kopp, G., Hase, F., Hochschild, G., Mikuteit, S., Raffalski, U., and Ruhnke, R.: Observation of unusual chlorine activation by ground-based infrared and microwave spectroscopy in the late Arctic winter 2000/01, Atmos. Chem. Phys., 6, 897–905, https://doi.org/10.5194/acp-6-897-2006, 2006.

Boone, C. D., Nassar, R., Walker, K. A., Rochon, Y., McLeod, S. D., Rinsland, C. P., and Bernath, P. F.: Retrievals for the atmospheric chemistry experiment Fourier-transform spectrometer, Appl. Opt., 44, 7218–7231, https://doi.org/10.1364/AO.44.007218, 2005.

Boone, C. D., Walker, K. A., and Bernath, P. F.: Version 3 Retrievals for the Atmospheric Chemistry Experiment Fourier Transform Spectrometer (ACE-FTS), in: ACE at 10: Solar Occultation Anthology, edited by: Bernath, P. F., A. Deepak Publishing, Hampton, Virg., 103–127, 2013.

Buchwitz, M., Schneising, O., Burrows, J. P., Bovensmann, H., Reuter, M., and Notholt, J.: First direct observation of the atmospheric $CO_2$ year-to-year increase from space, Atmos. Chem. Phys., 7, 4249–4256, https://doi.org/10.5194/acp-7-4249-2007, 2007.

Côté, J. S., Gravel, S., Méthot, A., Patoine, A., Roch, M., and Staniforth, A.: The operational CMC-MRB global environmental multiscale (GEM) model. Part I: Design considerations and formulation, Mon. Weather Rev., 126, 1373–1395, https://doi.org/10.1175/1520-0493(1998)126<1373:TOCMGE>2.0.CO;2, 1998.

de Mazière, M., Vigouroux, C., Bernath, P. F., Baron, P., Blumenstock, T., Boone, C., Brogniez, C., Catoire, V., Coffey, M., Duchatelet, P., Griffith, D., Hannigan, J., Kasai, Y., Kramer, I., Jones, N., Mahieu, E., Manney, G. L., Piccolo, C., Randall, C., Robert, C., Senten, C., Strong, K., Taylor, J., Tétard, C., Walker, K. A., and Wood, S.: Validation of ACE-FTS v2.2 methane profiles from the upper troposphere to the lower mesosphere, Atmos. Chem. Phys., 8, 2421–2435, https://doi.org/10.5194/acp-8-2421-2008, 2008.

Engel, A., Bönisch, H., Schwarzenberger, T., Haase, H.-P., Grunow, K., Abalichin, J., and Sala, S.: Long-term validation of ESA operational retrieval (version 6.0) of MIPAS Envisat vertical profiles of methane, nitrous oxide, CFC11, and CFC12 using balloon-borne observations and trajectory matching, Atmos. Meas. Tech., 9, 1051–1062, https://doi.org/10.5194/amt-9-1051-2016, 2016.

Errera, Q., Ceccherini, S., Christophe, Y., Chabrillat, S., Hegglin, M. I., Lambert, A., Ménard, R., Raspollini, P., Skachko, S., van Weele, M., and Walker, K. A.: Harmonisation and diagnostics of MIPAS ESA $CH_4$ and $N_2O$ profiles using data assimilation, Atmos. Meas. Tech., 9, 5895–5909, https://doi.org/10.5194/amt-9-5895-2016, 2016.

Fischer, H., Birk, M., Blom, C., Carli, B., Carlotti, M., von Clarmann, T., Delbouille, L., Dudhia, A., Ehhalt, D., Endemann, M., Flaud, J. M., Gessner, R., Kleinert, A., Koopman, R., Langen, J., López-Puertas, M., Mosner, P., Nett, H., Oelhaf, H., Perron, G., Remedios, J., Ridolfi, M., Stiller, G., and Zander, R.: MIPAS: an instrument for atmospheric and climate research, Atmos. Chem. Phys., 8, 2151–2188, https://doi.org/10.5194/acp-8-2151-2008, 2008.

Goldman, A., Paton-Walsh, C., Bell, W., Toon, G. C. andBlavier, J. F., Sen, B., Coffey, M. T., Hannigan, J. W., and Mankin, W. G.: Network for the detection of stratospheric change Fourier transform infrared intercomparison at Table Mountain Facility, November 1996, J. Geophys. Res., 104, 30481–30503, https://doi.org/10.1029/1999JD900879, 1999.

Hannigan, J. W., Coffey, M. T., and Goldman, A.: Semiautonomous FTS observation system for stratospheric and tropospheric gases, J. Atmos. Ocean. Tech., 26, 1814–1828, https://doi.org/10.1175/2009JTECHA1230.1, 2009.

Hase, F., Hannigan, J. W., Coffey, M. T., Goldman, A., Hopfner, M., Jones, N. B., Rinsland, C. P., and Wood, S. W.: Intercomparison of retrieval codes used for the analysis of high-resolution, ground-based FTIR measurements, J. Quant. Spectrosc. Ra., 87, 25–52, https://doi.org/10.1016/j.jqsrt.2003.12.008, 2004.

Holl, G., Walker, K. A., Conway, S., Saitoh, N., Boone, C. D., Strong, K., and Drummond, J. R.: Methane cross-validation between three Fourier transform spectrometers: SCISAT ACE-FTS, GOSAT TANSO-FTS, and ground-based FTS measurements in the Canadian high Arctic, Atmos. Meas. Tech., 9, 1961–1980, https://doi.org/10.5194/amt-9-1961-2016, 2016.

Ishida, H. and Nakajima, T. Y.: Development of an unbiased cloud detection algorithm for a spaceborne multispectral imager, J. Geophys. Res., 114, D07206, https://doi.org/10.1029/2008JD010710, 2009.

Ishida, H., Nakjima, T. Y., Yokota, T., Kikuchi, N., and Watanabe, H.: Investigation of GOSAT TANSO-CAI cloud screening ability through an intersatellite comparison, J. Appl. Meteorol. Climatol., 50, 1571–1586, https://doi.org/10.1175/2011JAMC2672.1, 2011.

Jin, J. J., Semeniuk, K., Beagley, S. R., Fomichev, V. I., Jonsson, A. I., McConnell, J. C., Urban, J., Murtagh, D., Manney, G. L., Boone, C. D., Bernath, P. F., Walker, K. A., Barret, B., Ricaud, P., and Dupuy, E.: Comparison of CMAM simulations of carbon monoxide (CO), nitrous oxide ($N_2O$), and methane ($CH_4$) with observations from Odin/SMR, ACE-FTS, and Aura/MLS, Atmos. Chem. Phys., 9, 3233–3252, 2009.

Kohlhepp, R., Ruhnke, R., Chipperfield, M. P., De Mazière, M., Notholt, J., Barthlott, S., Batchelor, R. L., Blatherwick, R. D., Blumenstock, T., Coffey, M. T., Demoulin, P., Fast, H., Feng, W., Goldman, A., Griffith, D. W. T., Hamann, K., Hannigan, J. W., Hase, F., Jones, N. B., Kagawa, A., Kaiser, I., Kasai, Y., Kirner, O., Kouker, W., Lindenmaier, R., Mahieu, E., Mittermeier, R. L., Monge-Sanz, B., Morino, I., Murata, I., Nakajima, H., Palm, M., Paton-Walsh, C., Raffalski, U., Reddmann, T., Rettinger, M., Rinsland, C. P., Rozanov, E., Schneider, M., Senten, C., Servais, C., Sinnhuber, B.-M., Smale, D., Strong, K., Sussmann, R., Taylor, J. R., Vanhaelewyn, G., Warneke, T., Whaley, C., Wiehle, M., and Wood, S. W.: Observed and simulated time evolution of HCl, $ClONO_2$, and HF total column abundances, Atmos. Chem. Phys., 12, 3527–3556, https://doi.org/10.5194/acp-12-3527-2012, 2012.

Kurylo, M. J. and Zander, R.: The NDSC–Its status after 10 years of operation, in: Proc. 19th Quadrennial Ozone Symp., 167–168, 2000.

Kuze, A., Suto, H., Nakajima, M., and Hamazaki, T.: Thermal and near infrared sensor for carbon observation Fourier-transform spectrometer on the Greenhouse Gases Observing Satellite for greenhouse gases monitoring, Appl. Opt., 48, 6716, https://doi.org/10.1364/AO.48.006716, 2009.

Kuze, A., Suto, H., Shiomi, K., Urabe, T., Nakajima, M., Yoshida, J., Kawashima, T., Yamamoto, Y., Kataoka, F., and Buijs, H.: Level 1 algorithms for TANSO on GOSAT: processing and on-orbit calibrations, Atmos. Meas. Tech., 5, 2447–2467, https://doi.org/10.5194/amt-5-2447-2012, 2012.

Kuze, A., Suto, H., Shiomi, K., Kawakami, S., Tanaka, M., Ueda, Y., Deguchi, A., Yoshida, J., Yamamoto, Y., Kataoka, F., Taylor, T. E., and Buijs, H. L.: Update on GOSAT TANSO-FTS performance, operations, and data products after more than 6 years in space, Atmos. Meas. Tech., 9, 2445–2461, https://doi.org/10.5194/amt-9-2445-2016, 2016.

Laeng, A., Plieninger, J., von Clarmann, T., Grabowski, U., Stiller, G., Eckert, E., Glatthor, N., Haenel, F., Kellmann, S., Kiefer, M., Linden, A., Lossow, S., Deaver, L., Engel, A., Hervig, M., Levin, I., McHugh, M., Noël, S., Toon, G., and Walker, K.: Validation of MIPAS IMK/IAA methane profiles, Atmos. Meas. Tech., 8, 5251–5261, https://doi.org/10.5194/amt-8-5251-2015, 2015.

Maksyutov, S., Patra, P. K., Onishi, R. A. S. T., and T., N.: NIES/FRCGC global atmospheric tracer transport model: Description, validation, and surface sources and sinks inversion, J. Earth Simul., 9, 3–18, 2008.

Notholt, J., Toon, G. C., Stordal, F., S., S., Schmidbauer, N., Becker, E., Meier, A., and Sen, B.: Seasonal variations of atmospheric trace gases in the high Arctic at 79° N, J. Geophys. Res., 102, 12855–12861, https://doi.org/10.1029/97JD00337, 1997.

Payan, S., Camy-Peyret, C., Oelhaf, H., Wetzel, G., Maucher, G., Keim, C., Pirre, M., Huret, N., Engel, A., Volk, M. C., Kuellmann, H., Kuttippurath, J., Cortesi, U., Bianchini, G., Mencaraglia, F., Raspollini, P., Redaelli, G., Vigouroux, C., de Mazière, M., Mikuteit, S., Blumenstock, T., Velazco, V., Notholt, J., Mahieu, E., Duchatelet, P., Smale, D., Wood, S., Jones, N., Piccolo, C., Payne, V., Bracher, A., Glatthor, N., Stiller, G., Grunow, K., Jeseck, P., Te, Y., and Butz, A.: Validation of version-4.61 methane and nitrous oxide observed by MIPAS, Atmos. Chem. Phys., 9, 413–442, https://doi.org/10.5194/acp-9-413-2009, 2009.

Picone, J. M., Hedin, A. E., Drob, D. P., and Aikin, A. C.: NRLMSISE-00 empirical model of the atmosphere: Statistical comparisons and scientific issues, J. Geophys. Res., 107, 1468, https://doi.org/10.1029/2002JA009430, 2002.

Plieninger, J., von Clarmann, T., Stiller, G. P., Grabowski, U., Glatthor, N., Kellmann, S., Linden, A., Haenel, F., Kiefer, M., Höpfner, M., Laeng, A., and Lossow, S.: Methane and nitrous oxide retrievals from MIPAS-ENVISAT, Atmos. Meas. Tech., 8, 4657–4670, https://doi.org/10.5194/amt-8-4657-2015, 2015.

Plieninger, J., Laeng, A., Lossow, S., von Clarmann, T., Stiller, G. P., Kellmann, S., Linden, A., Kiefer, M., Walker, K. A., Noël, S., Hervig, M. E., McHugh, M., Lambert, A., Urban, J., Elkins, J. W., and Murtagh, D.: Validation of revised methane and nitrous oxide profiles from MIPAS-ENVISAT, Atmos. Meas. Tech., 9, 765–779, https://doi.org/10.5194/amt-9-765-2016, 2016.

Pougatchev, N. S., Connor, B. J., and Rinsland, C. P.: Infrared measurements of the ozone vertical distribution above Kitt Peak, J. Geophys. Res., 100, 16689–16697, https://doi.org/10.1029/95JD01296, 1995.

Raspollini, P., Belotti, C., Burgess, A., Carli, B., Carlotti, M., Ceccherini, S., Dinelli, B. M., Dudhia, A., Flaud, J.-M., Funke,

B., Höpfner, M., López-Puertas, M., Payne, V., Piccolo, C., Remedios, J. J., Ridolfi, M., and Spang, R.: MIPAS level 2 operational analysis, Atmos. Chem. Phys., 6, 5605–5630, https://doi.org/10.5194/acp-6-5605-2006, 2006.

Raspollini, P., Carli, B., Carlotti, M., Ceccherini, S., Dehn, A., Dinelli, B. M., Dudhia, A., Flaud, J.-M., López-Puertas, M., Niro, F., Remedios, J. J., Ridolfi, M., Sembhi, H., Sgheri, L., and von Clarmann, T.: Ten years of MIPAS measurements with ESA Level 2 processor V6 – Part 1: Retrieval algorithm and diagnostics of the products, Atmos. Meas. Tech., 6, 2419–2439, https://doi.org/10.5194/amt-6-2419-2013, 2013.

Raspollini, P., Arnone, E., Barbara, F., Carli, B., Castelli, E., Ceccherini, S., Dinelli, B. M., Dudhia, A., Kiefer, M., Papandrea, E., and Ridolfi, M.: Comparison of the MIPAS products obtained by four different level 2 processors, Ann. Geophys., 56, https://doi.org/10.4401/ag-6338, 2014.

Remedios, J. J., Leigh, R. J., Waterfall, A. M., Moore, D. P., Sembhi, H., Parkes, I., Greenhough, J., Chipperfield, M. P., and Hauglustaine, D.: MIPAS reference atmospheres and comparisons to V4.61/V4.62 MIPAS level 2 geophysical data sets, Atmos. Chem. Phys., 7, 9973–10017, https://doi.org/10.5194/acpd-7-9973-2007, 2007.

Rodgers, C. D. and Connor, B. J.: Intercomparison of remote sounding instruments, J. Geophys. Res., 108, 2156–2202, https://doi.org/10.1029/2002JD002299, 2003.

Rothman, L. S., Rinsland, C. P., Goldman, A., Massie, S. T., Edwards, D. P., Flaud, J.-M., Perrin, A., Camy-Peyret, C., Dana, V., Mandin, J.-Y., Schroeder, J., McCann, A., Gamache, R. R., Wattson, R. B., Yoshino, K., Chance, K., Jucks, K., Brown, L. R., Nemtchinov, V., and Varanasi, P.: The HITRAN Molecular Spectroscopic Database and HAWKS (HITRAN Atmospheric Workstation): 1996 Edition, J. Quant. Spectrosc. Ra., 60, 665–710, https://doi.org/10.1016/S0022-4073(98)00078-8, 1998.

Rothman, L. S., Jacquemart, D., Barbe, A., Chris Benner, D., Birk, M., Brown, L. R., Carleer, M. R., Chackerian, C., Chance, K., Coudert, L. H., Dana, V., Devi, V. M., Flaud, J.-M., Gamache, R. R., Goldman, A., Hartmann, J.-M., Jucks, K. W., Maki, A. G., Mandin, J.-Y., Massie, S. T., Orphal, J., Perrin, A., Rinsland, C. P., Smith, M. A. H., Tennyson, J., Tolchenov, R. N., Toth, R. A., Vander Auwera, J., Varanasi, P., and Wagner, G.: The HITRAN 2004 molecular spectroscopic database, J. Quant. Spectrosc. Ra., 96, 139–204, https://doi.org/10.1016/j.jqsrt.2004.10.008, 2005.

Rothman, L. S., Gordon, I. E., Barbe, A., Benner, D. C., Bernath, P. F., Birk, M., Boudon, V., Brown, L. R., Campargue, A., Champion, J.-P., Chance, K., Coudert, L. H., Dana, V., Devi, V. M., Fally, S., Flaud, J.-M., Gamache, R. R., Goldman, A., Jacquemart, D., Kleiner, I., Lacome, N., Lafferty, W. J., Mandin, J.-Y., Massie, S. T., Mikhailenko, S. N., Miller, C. E., Moazzen-Ahmadi, N., Naumenko, O. V., Nikitin, A. V., Orphal, J., Perevalov, V. I., Perrin, A., Predoi-Cross, A., Rinsland, C. P., Rotger, M., Šimečková, M., Smith, M. A. H., Sung, K., Tashkun, S. A., Tennyson, J., Toth, R. A., Vandaele, A. C., and Vander Auwera, J.: The HITRAN 2008 molecular spectroscopic database, J. Quant. Spectrosc. Ra., 110, 533–572, https://doi.org/10.1016/j.jqsrt.2009.02.013, 2009.

Rothman, L. S., Gordon, I. E., Babikov, Y., Barbe, A., Chris Benner, D., Bernath, P. F., Birk, M., Bizzocchi, L., Boudon, V., Brown, L. R., Campargue, A., Chance, K., Cohen, E. A., Coudert, L. H., Devi, V. M., Drouin, B. J., Fayt, A., Flaud, J.-M., Gamache, R. R., Harrison, J. J., Hartmann, J.-M., Hill, C., Hodges, J. T., Jacquemart, D., Jolly, A., Lamouroux, J., Le Roy, R. J., Li, G., Long, D. A., Lyulin, O. M., Mackie, C. J., Massie, S. T., Mikhailenko, S., Müller, H. S. P., Naumenko, O. V., Nikitin, A. V., Orphal, J., Perevalov, V., Perrin, A., Polovtseva, E. R., Richard, C., Smith, M. A. H., Starikova, E., Sung, K., Tashkun, S., Tennyson, J., Toon, G. C., Tyuterev, V. G., and Wagner, G.: The HITRAN2012 molecular spectroscopic database, J. Quant. Spectrosc. Ra., 130, 4–50, https://doi.org/10.1016/j.jqsrt.2013.07.002, 2013.

Saeki, T., Saito, R., Belikov, D., and Maksyutov, S.: Global high-resolution simulations of $CO_2$ and $CH_4$ using a NIES transport model to produce a priori concentrations for use in satellite data retrievals, Geosci. Model Dev., 6, 81–100, https://doi.org/10.5194/gmd-6-81-2013, 2013.

Saitoh, N., Imasu, R., Ota, Y., and Niwa, Y.: $CO_2$ retrieval algorithm for the thermal infrared spectra of the Greenhouse Gases Observing Satellite: Potential of retrieving $CO_2$ vertical profile from high-resolution FTS sensor, J. Geophys. Res., 114, D17305, https://doi.org/10.1029/2008JD011500, 2009.

Saitoh, N., Kimoto, S., Sugimura, R., Imasu, R., Kawakami, S., Shiomi, K., Kuze, A., Machida, T., Sawa, Y., and Matsueda, H.: Algorithm update of the GOSAT/TANSO-FTS thermal infrared $CO_2$ product (version 1) and validation of the UTLS $CO_2$ data using CONTRAIL measurements, Atmos. Meas. Tech., 9, 2119–2134, https://doi.org/10.5194/amt-9-2119-2016, 2016.

Schneider, M., Blumenstock, T., Chipperfield, M., Hase, F., Kouker, W., Reddmann, T., Ruhnke, R., Cuevas, E., and Fischer, H.: Subtropical trace gas profiles determined by ground-based FTIR spectroscopy at Izaña (28° N, 16° W): Five year record, error analysis, and comparison with 3-D CTMs, Atmos. Chem. Phys., 5, 153–167, https://doi.org/10.5194/acp-5-153-2005, 2005.

Senten, C., de Mazière, M., Dils, B., Hermans, C., Kruglanski, M., Neefs, E., Scolas, F., Vandaele, A. C., Vanhaelewyn, G., Vigouroux, C., Carleer, M., Coheur, P. F., Fally, S., Barret, B., Baray, J. L., Delmas, R., Leveau, J., Metzger, J. M., Mahieu, E., Boone, C. D., Walker, K. A., Bernath, P. F., and Strong, K.: Technical Note: New ground-based FTIR measurements at Ile de La Réunion: observations, error analysis, and comparisons with independent data, Atmos. Chem. Phys., 8, 3483–3508, https://doi.org/10.5194/acp-8-3483-2008, 2008.

Sepúlveda, E., Schneider, M., Hase, F., García, O. E., Gomez-Pelaez, A., Dohe, S., Blumenstock, T., and Guerra, J. C.: Long-term validation of tropospheric column-averaged $CH_4$ mole fractions obtained by mid-infrared ground-based FTIR spectrometry, Atmos. Meas. Tech., 5, 1425–1441, https://doi.org/10.5194/amt-5-1425-2012, 2012.

Sepúlveda, E., Schneider, M., Hase, F., Barthlott, S., Dubravica, D., García, O. E., Gomez-Pelaez, A., González, Y., Guerra, J. C., Gisi, M., Kohlhepp, R., Dohe, S., Blumenstock, T., Strong, K., Weaver, D., Palm, M., Sadeghi, A., Deutscher, N. M., Warneke, T., Notholt, J., Jones, N., Griffith, D. W. T., Smale, D., Brailsford, G. W., Robinson, J., Meinhardt, F., Steinbacher, M., Aalto, T., and Worthy, D.: Tropospheric $CH_4$ signals as observed by NDACC FTIR at globally distributed sites and comparison to GAW surface in situ measurements, Atmos. Meas. Tech., 7, 2337–2360, https://doi.org/10.5194/amt-7-2337-2014, 2014.

Sheese, P., Walker, K., and Boone, C.: Atmospheric pseudo-retrievals for averaging kernel and total uncertainty characterization for ACE-FTS level 2 (PRAKTICAL) data, in: EGU General Assembly, vol. 18 of EGU General Assembly, p. 17582, 2016.

Sheese, P. E., Boone, C. D., and Walker, K. A.: Detecting physically unrealistic outliers in ACE-FTS atmospheric measurements, Atmos. Meas. Tech., 8, 741–750, https://doi.org/10.5194/amt-8-741-2015, 2015.

Sussmann, R. and Schäfer, K.: Infrared spectroscopy of tropospheric trace gases: combined analysis of horizontal and vertical column abundances, Appl. Opt., 36, 735–741, https://doi.org/10.1364/AO.36.000735, 1997.

Sussmann, R., Forster, F., Rettinger, M., and Jones, N.: Strategy for high-accuracy-and-precision retrieval of atmospheric methane from the mid-infrared FTIR network, Atmos. Meas. Tech., 4, 1943–1964, https://doi.org/10.5194/amt-4-1943-2011, 2011.

Sussmann, R., Ostler, A., Forster, F., Rettinger, M., Deutscher, N. M., Griffith, D. W. T., Hannigan, J. W., Jones, N., and Patra, P. K.: First intercalibration of column-averaged methane from the Total Carbon Column Observing Network and the Network for the Detection of Atmospheric Composition Change, Atmos. Meas. Tech., 6, 397–418, https://doi.org/10.5194/amt-6-397-2013, 2013.

Toon, G. C., Blavier, J.-F., Sung, K., Rothman, L. S., and E. Gordon, I.: HITRAN spectroscopy evaluation using solar occultation FTIR spectra, J. Quant. Spectrosc. Ra., 182, 324–336, https://doi.org/10.1016/j.jqsrt.2016.05.021, 2016.

Vincenty, T.: Direct and Inverse Solutions of Geodesics on the Ellipsoid with application of nested equations, Surv. Rev., 23, 88–93, https://doi.org/10.1179/sre.1975.23.176.88, 1975.

von Clarmann, T., Höpfner, M., Kellmann, S., Linden, A., Chauhan, S., Funke, B., Grabowski, U., Glatthor, N., Kiefer, M., Schieferdecker, T., Stiller, G. P., and Versick, S.: Retrieval of temperature, $H_2O$, $O_3$, $HNO_3$, $CH_4$, $N_2O$, $ClONO_2$ and ClO from MIPAS reduced resolution nominal mode limb emission measurements, Atmos. Meas. Tech., 2, 159–175, https://doi.org/10.5194/amt-2-159-2009, 2009.

Waymark, C., Walker, K. A., Boone, C. D., and Bernath, P. F.: ACE-FTS version 3.0 data set: validation and data processing update, Ann. Geophys., 56, https://doi.org/10.4401/ag-6339, 2013.

Wiacek, A., Taylor, J. R., Strong, K., Saari, R., Kerzenmacher, T., Jones, N. B., and Griffith, D. W. T.: Ground-Based solar absorption FTIR spectroscopy: characterization of retrievals and first results from a novel optical design instrument at a New NDACC Complementary Station, J. Atmos. Ocean. Tech., 24, 432–448, https://doi.org/10.1175/JTECH1962.1, 2007.

Wood, S. W., Bodeker, G. E., Boyd, I. S., Jones, N. B., Connor, B. J., Johnston, P. V., Matthews, W. A., Nichol, S. E., Murcray, F. J., Nakajima, H., and Sasano, Y.: Validation of version 5.20 ILAS $HNO_3$, $CH_4$, $N_2O$, $O_3$, and $NO_2$ using ground-based measurements at Arrival Heights and Kiruna, J. Geophys. Res., 107, 8208, https://doi.org/10.1029/2001JD000581, 2002.

Yokota, T., Yoshida, Y., Eguchi, N., Ota, Y., Tanaka, T., Watanabe, H., and Maksyutov, S.: Global Concentrations of $CO_2$ and $CH_4$ Retrieved from GOSAT: First Preliminary Results, Sci. Online Lett. Atmos., 5, 160–163, https://doi.org/10.2151/sola.2009-041, 2009.

Zander, R., Mahieu, E., Demoulin, P., Duchatelet, P., Roland, G., Servais, C., de Mazière, M., Reimann, S., and Rinsland, C. P.: Our changing atmosphere: evidence based on long-term infrared solar observations at the Jungfraujoch since 1950, Sci. Total Environ., 391, 184–195, https://doi.org/10.1016/j.scitotenv.2007.10.018, 2008.

Zou, M., Xiong, X., Saitoh, N., Warner, J., Zhang, Y., Chen, L., Weng, F., and Fan, M.: Satellite observation of atmospheric methane: intercomparison between AIRS and GOSAT TANSO-FTS retrievals, Atmos. Meas. Tech., 9, 3567–3576, https://doi.org/10.5194/amt-9-3567-2016, 2016.